NASA Technical Paper 3387

Numerical and Experimental Analyses of the Radiant Heat Flux Produced by Quartz Heating Systems

Travis L. Turner and Robert L. Ash

March 1994

NASA Technical Paper 3387

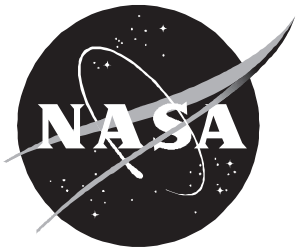

Numerical and Experimental Analyses of the Radiant Heat Flux Produced by Quartz Heating Systems

Travis L. Turner
Langley Research Center • Hampton, Virginia

Robert L. Ash
Old Dominion University • Norfolk, Virginia

National Aeronautics and Space Administration
Langley Research Center • Hampton, Virginia 23681-0001

March 1994

National Aeronautics and
Space Administration
Code JTT
Washington, D.C.
20546-0001

Official Business
Penalty for Private Use, $300

B U L K R A T E
POSTAGE & FEES PAID
NASA Permit No. G-27

Postmaster: If undeliverable (Section 158 Postal Manual) Do Not Return

Summary

A method is developed for predicting the radiant heat flux distribution produced by tungsten filament, tubular fused-quartz envelope heating systems with reflectors. The method is an application of Monte Carlo simulation, which takes the form of a random walk or ray tracing scheme. The method is applied to four systems of increasing complexity, including a single lamp without a reflector, a single lamp with a flat reflector, a single lamp with a parabolic reflector, and up to six lamps in a six-lamp contoured-reflector heating unit. The application of the Monte Carlo method to the simulation of the thermal radiation generated by these systems is discussed. The procedures for numerical implementation are also presented.

Experiments were conducted to study these quartz heating systems and to acquire measurements of the corresponding empirical heat flux distributions for correlation with analysis. The experiments were conducted such that several complicating factors could be isolated and studied sequentially. Comparisons of the experimental results with analysis are presented and discussed. Good agreement between the experimental and simulated results was obtained in all cases.

This study shows that this method can be used to analyze very complicated quartz heating systems and can account for factors such as spectral properties, specular reflection from curved surfaces, source enhancement due to reflectors and/or adjacent sources, and interaction with a participating medium in a straightforward manner.

Introduction

Purpose of Study

Prospective advanced aircraft, such as the High-Speed Civil Transport (HSCT) and the National Aerospace Plane (NASP), will be subject to intense acoustic and thermal loads. Acoustic loads encountered in a typical flight envelope of a NASP-type vehicle are projected to be on the order of 180 dB with thermal loads reaching 57 000 W/cm^2, which can drive skin temperatures to 1700°C and the structural response into the nonlinear regime. Analysis of such structures is certain to require a multidisciplinary approach. Such intense loading in conjunction with strict weight limitations will require the use of advanced materials (e.g., composites) and advanced structural concepts, such as integrally cooled skin sections. Thus, extensive theoretical and experimental analyses of prospective structures will be required to ensure structural integrity.

A very large percentage of the necessary tests will involve simulation of portions of the flight environment (e.g., thermal-acoustic tests). Tungsten filament, tubular fused-quartz envelope (halogen type) heating systems, consisting of multiple lamps and reflector(s), are known to be highly desirable for these applications because of their load generation capability, efficiency, and controllability (ref. 1). The nature of the heat transfered by these systems (radiant transfer) is also advantageous, since it is not affected by a convective flow field. On the other hand, the high heating rates, control methods, and relatively large target area associated with tests in representative facilities render iterative design and local measurement of the radiant heat distribution totally inadequate. Thus, there is a need for a method of predicting the distribution of radiant energy produced by these quartz heating systems. Such an analysis would also be an indespensible aid in designing an optimal heating system for particular applications. In the remainder of this paper, heating systems involving lamp elements with tubular fused-quartz envelopes will be referred to as *quartz heating systems*. The vitreous silica used in making the lamp envelopes and heater windows will be referred to as *fused-quartz* or *quartz*.

Literature Review

Quartz heating systems involving reflectors have been in use for approximately 20 years (ref. 1). The inherent properties of these systems, and recent improvements, have kept them in the forefront of thermal load generation methods for a wide variety of applications. However, theoretical analysis of quartz heating systems has been sparse and practically undocumented. No analysis of complex systems involving curved reflectors and multiple lamps is known to the authors.

Previous work was done to predict the radiant heat flux produced on a planar surface by a single tubular quartz heater with and without the effects of reflectors (refs. 2–4). Those analyses were based upon a classical method that required extensive simplifying assumptions as follows: (1) The surface of the quartz tube is considered to be the sole radiation source, rather than considering any interactions between the filament and the quartz. (2) The radiant energy is assumed to be uniformly distributed over the lamp surface. (3) The radiant intensity at the quartz surface is assumed to be independent of direction. (4) The fraction of the irradiation absorbed, transmitted, and reflected by a surface is independent of direction (diffuse). (5) The fraction of the irradiation absorbed, transmitted, and reflected by a

surface is independent of wavelength (gray). (6) Radiation reflected back to the source is lost.

Assumptions 1, 2, and 3 allow the intensity of the emitted radiation from the quartz tube to be related to the emissive power of the lamp. Thus, the radiant heat flux on any surface may be derived and related to the power of the lamp based upon the definition and integration of a differential view factor. Furthermore, reflected contributions from a flat reflector may be taken into account by superimposing diffuse and specular components. Diffuse components were treated by defining a diffusely reflected radiation intensity, followed by integration of the differential view factor between the reflector and the test surface. Specular reflection was treated by adding the contribution from a virtual lamp located at the specular image in the flat reflector.

It is apparent from the above discussion that this classical analysis of the reflected contributions has severe limitations. Namely, curved reflectors pose insurmountable difficulties, since a specular view factor from a curved surface is not known, and inclusion of multiple reflections is approximate and extremely tedious. Thus, it was found that this classical analysis technique is applicable to very few, relatively simple cases involving reflectors. Therefore, with the understanding that a useful analytical model requires capability (at a minimum) for multiple reflection and specular reflection from curved surfaces, it was decided that a numerical technique should be adopted. Since it is somewhat common to think of radiant transfer in terms of energy bundles or photons, a statistical method seems appropriate for analysis of complex systems. One statistical method particularly suited to particle diffusion and radiation problems is the Monte Carlo method.

Literature pertaining to the origination and general development of the Monte Carlo method is obtainable. Some particularly useful examples include references 5–7. However, these documents do not discuss the simulation of thermal radiation. Some additional detail may be found in reference 8.

Numerous works dealing with the application of Monte Carlo simulation to thermal radiation have appeared since the publication of the above benchmark documents (refs. 5 and 6). The problems treated in these publications are somewhat variable, but the procedures are similar. Howell and Perlmutter (ref. 9) used a Monte Carlo simulation technique to study the radiant heat transfer through a nonisothermal absorbing and emitting gray gas between gray walls. Several papers (refs. 10–12) followed this effort, extending the analysis to cylindrical geometry, temperature-dependent properties, and concurrent convective fields (rocket nozzles). Some of the basic concepts in these references are developed in a more general manner in references 13 and 14. A related application was documented by Murakami (ref. 15), where the temperature field between nonisothermal gray walls was assumed two-dimensional. Similar approaches were used by Weiner et al. (ref. 16), Corlett (ref. 17), Toor and Viskanta (ref. 18), Mahan and Eskin (ref. 19), and Hoff and Janni (ref. 20) to calculate approximate radiant exchange view factors for a number of simple geometries.

Chou (ref. 21) developed an *importance sampling* procedure for a Monte Carlo simulation of thermal radiation and optical systems. This procedure was developed to reduce the computational burden in systems that exhibit pertinent processes of small probability (e.g., estimation of the energy flux through a small aperture due to radiation from a large source). Morris et al. (ref. 22) documented a study of radiative transfer through solar collectors where a Monte Carlo approach was adapted to estimate the radiative properties of glass honeycomb. This work includes an effort to account for polarization and scattering effects.

Naraghi and Chung (ref. 23) applied a related stochastic method for calculation of radiant interchange in an enclosure without a participating medium. This approach is based upon Markov chain theory, which forces the use of an approximation for analysis of specularly reflecting surfaces. Another alternative method was implemented by Rasmussen et al. (ref. 24) that employs Gauss-Legendre quadrature over discrete elements. These elements make up a geometric model of the surfaces in the system. This method is also restrictive, since it requires constant surface properties, which are independent of wavelength, and it cannot treat specular reflection.

Scope of the Present Study

The quartz heating systems incorporated in most practical applications are complex. Complicating factors such as curved reflectors and multiple lamp interactions present severe difficulties for analysis. Therefore, an attempt was made to develop a theoretical model through correlation with experiments of increasing complexity, which could be used to analyze and design complex heating systems. This procedure was intended to isolate various phenomena and include them in a more predictable sequential manner.

The systems discussed in this study include a single lamp without a reflector, a single lamp with a flat reflector, a single lamp with a parabolic reflector,

a single lamp located at various positions in a six-lamp heating unit, and a full six-lamp heating unit. Successful analysis of the six-lamp heating unit is an important milestone, and an important goal of this work, since this has implications for analysis of more complicated systems consisting of arrays of multilamp units.

Several phenomena common to thermal radiation transport will be neglected in the ensuing discussions. These may be summarized as follows. The gaseous environment surrounding and within the quartz envelope of a lamp is treated as a nonparticipating medium. The coiled tungsten filament is treated as a diffusely radiating cylinder of diameter equal to the coil diameter. Higher order effects such as scattering and birefringence are neglected. Polarization induced by any process (absorption, reflection, scattering, and birefringence) associated with the quartz is neglected. The quartz tube is treated as a partially reflecting, transmitting, and absorbing medium with specular interfaces. Metallic reflector surfaces are assumed to reflect radiant energy via additive specular and diffuse components. All cases are restricted to steady-state conditions.

The general simulation method is reduced to the specific applications in thermal radiation transfer. Simulation techniques for processes common to thermal radiation systems are introduced. The probability distribution functions necessary for the simulation of thermal radiation are developed and related to the simulation procedure. The model of the physical system is discussed in some detail. Gross spectral properties of the quartz used in the lamp envelopes are discussed. The effect of these spectral characteristics on the trajectory of participating energy bundles is determined. The analytical tools employed in modeling the interface and bulk processes of the quartz are developed. The interaction of bundles with other surfaces in the system is discussed, with particular emphasis on the manner in which the statistical results are normalized.

Wavelength selection for energy bundles emitted by a source from the appropriate Planckian distribution is presented. The spectral and directional radiative properties of the quartz envelopes are derived from the governing analytical models. The analytic geometry formulations employed for bundle incidence and reflection processes are developed for the general case. In particular, the equations governing the location of bundle incidence and reflected trajectories are derived. A flow chart exemplifying the simulation procedure for the relatively simple case of a single lamp with a flat reflector is presented.

The experimental apparatus, which was constructed to study the radiant heat flux distributions generated in a plane by the various heating systems, is described. The geometry and other quantities pertinent to each heating system and support structure are described in detail. The procedures employed in preparing for and executing a representative experiment are depicted.

The measured radiant heat flux distributions in the test plane, parallel to the two axes of each heating system, are compared with the simulated distributions. Observations on the validity of some theoretical assumptions and uncertainties in the experimental data are discussed. The effects of multilamp interactions are observed and investigated experimentally. The improvements in the simulated distributions generated by inclusion of several higher order modeling concepts are examined by suppressing selected phenomena independently. The effects of adding a quartz window and air cooling in a multilamp system are quantified and correlated with appropriate simulation models. Finally, a summary of this study and discussions on the capabilities and limitations of this work are presented.

Symbols

A	surface area, cm^2
a_{ij}	coordinate transformation direction cosines
a_1, a_2, a_3	emitted trajectory direction cosines
$\tilde{a}_1, \tilde{a}_2, \tilde{a}_3$	reflected trajectory direction cosines
b_{mn}	statistical event counter for bin (m, n)
c	speed of light, m/s; various constants
F	view factor; probability of incidence
$F(x)$	probability distribution function of x
$f(x)$	probability density of random variable x
H	height dimension
h	Planck's constant, J-s; height dimension
I	radiant intensity, W/cm^2-sr
k	Boltzmann's constant, J/K
L	lamp lighted length
$\overline{L}$	vector representation of a line
m	parabolic reflector dimension

N	sample population size
$\overline{N}$	vector normal to a plane
n	energy bundle counting integer; parabolic reflector dimension
$\hat{n}$	unit normal vector
Q	heating rate or radiative power, W
Q'	differential area heating rate, W
q	heat flux, W/cm^2
R	uniformly distributed random variable
r	radial distance
$\overline{S}$	vector representation of a surface
s	distance
T	source absolute temperature, K or °R
$\hat{u}$	unit trajectory vector
u_i	trajectory components
w	width dimension
x, y, z	position coordinates
α	absorptivity; geometric constant
β, γ	geometric constants
ϵ	surface emissivity
η	refractive index
η^*	complex refractive index
θ	angle of incidence
κ	absorptive index
λ	radiation wavelength, μm
ν	absorption coefficient
ξ	dummy integration variable
ρ	surface reflectivity
σ	Stefan-Boltzmann constant, 5.67×10^{-8} W/m^2-K^4
τ	transmissivity
ϕ	angle of refraction
Ω	solid angle

Subscripts:

b	pertaining to a black body
d	diffuse component
g	gas property
i	array index; denoting an incident quantity
j, k	array index
l	pertaining to a lamp
m	array index; maximum value of a variable
n	array index; normal (perpendicular) component
p	parallel component
q	quartz property
s	related to a surface, source, or specular component
t	total property
λ	spectrally dependent variable
ρ	related to surface reflectivity
0	initial or reference quantity

Monte Carlo Application

The natural *particle* for simulation of thermal radiation is a photon. However, the energy of a photon depends upon its wavelength. In order to avoid this complication, a *photon bundle* is chosen as the "model particle." Thus, each photon bundle comprises a varying number of photons of the particular wavelength, in order to produce a standard unit of energy for each photon bundle. In practice, this clarification becomes transparent, but it does introduce the basic modeling considerations in a consistent manner. It is noted that the term photon bundle will be designated simply as *bundle* or *energy bundle* throughout the following discussions.

Energy bundles are "emitted" at random from heated surfaces in the simulation model. Using random numbers, a surface location for energy emission can be selected, and then another random number can be used to assign a wavelength. Subsequently, random numbers can be used to assign a direction of departure for the energy bundle. By incorporating distribution functions, uniformly distributed random numbers can be "mapped" into nonuniform distributions to model realistic physical processes. Furthermore, by tracing the path of the emitted energy bundle, additional random numbers can be used to approximate transmission, reflection, or absorption when the path of the energy bundle intersects a surface. By developing appropriate distribution functions, the complete process can be simulated by repeated use of the technique (refs. 13 and 16).

The applications of the Monte Carlo method discussed here will be limited to cases where the source and emission distributions are assumed to be uniform (assumptions 2 and 3 from the classical analyses (refs. 2–4) have been retained). These assumptions may be relaxed readily in simulation theory (refs. 13 and 18), but they are retained here, since theoretical arguments permit them (see ref. 4), and the necessary distribution functions are not known. Attempts at experimental correlation revealed various model refinement requirements, beyond inclusion of multiple reflections and specular reflection from a curved surface. The required refinements were due primarily to the sensitivity of reflective systems to geometry and source energy distributions. Details on the general Monte Carlo methodology and statistical basis may be found elsewhere (refs. 5–8). Reference 8 may be consulted for a more informative discussion of the numerical implementation.

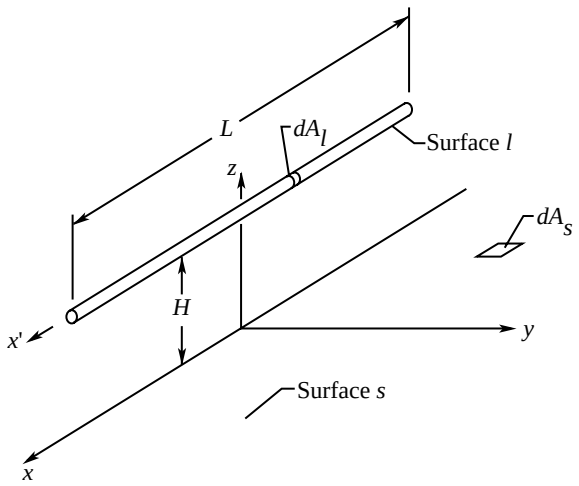

Figure 1. Coordinate system and relevant dimensions for radiation from a quartz lamp.

Distribution Functions

Monte Carlo simulations utilize probability distribution functions to model complex physical phenomena by mapping a uniformly distributed random variable into appropriate nonuniform distributions representing the physical phenomena. By modeling all aspects of a complex physical process in this manner, it is possible to simulate the process. However, since the Monte Carlo simulation replaces classical analytical techniques with probabilistic results, a large population of simulation trials must be produced to yield distribution results that converge toward the actual physical system.

Some of the distribution functions necessary for the construction of an energy bundle history may be inferred directly from the physical phenomena. However, in general, they are not intuitive and must be deduced from the classical governing equations, where the statistical basis of the Monte Carlo method will be utilized.

The source distributions that will be considered in this analysis are assumed to be uniform (i.e., spatially constant source temperature and emissivity). Thus, the analysis must ensure that the probability of emission is equal at every surface position on the source. This is accomplished through selection of position coordinates, belonging to the source surface, from uniformly distributed random variables, with limits corresponding to the source dimensions. Sufficient repetition of this process ensures that the simulated source distribution will be, for all practical purposes, uniform. Various algorithms for random number generation are generally available with popular software packages. However, Park (ref. 25) found that most are unsatisfactory. Therefore, a *minimal standard* generator, recommended by Park and based on Lehmer's algorithm, was employed in these applications. A discussion of this generator may be found in reference 8, and further information may be found in reference 25. It is reiterated that various other physical processes have been simulated assuming random selection of a number from a uniform distribution within the interval $(0, 1)$. In all cases, the generator based on Lehmer's algorithm is the implied method for making the selection.

Simulation of thermal radiation requires distribution functions to simulate diffuse surface events. Since it is assumed that the source is emitting diffusely, emission will be used as a means of demonstrating the necessary distribution functions. The energy emitted by the cylindrical surface l to the surrounding space may be discretized as a number (N_l) of energy bundles, each with equal energy. (See fig. 1.) Since the source distribution is assumed uniform, a differential portion (dA_l) of the radiating surface may be considered. Denoting the number of bundles emitted by surface element dA_l that are incident upon the test surface element dA_s by N_{ls}, the view factor from dA_l to dA_s may be approximated by

$$F_{ls} \approx \frac{N_{ls}}{N_l} \tag{1}$$

for large N_l (ref. 16). Note the similarity of this relation to the relative frequency of bundles striking the surface s, that is, the probability that a bundle,

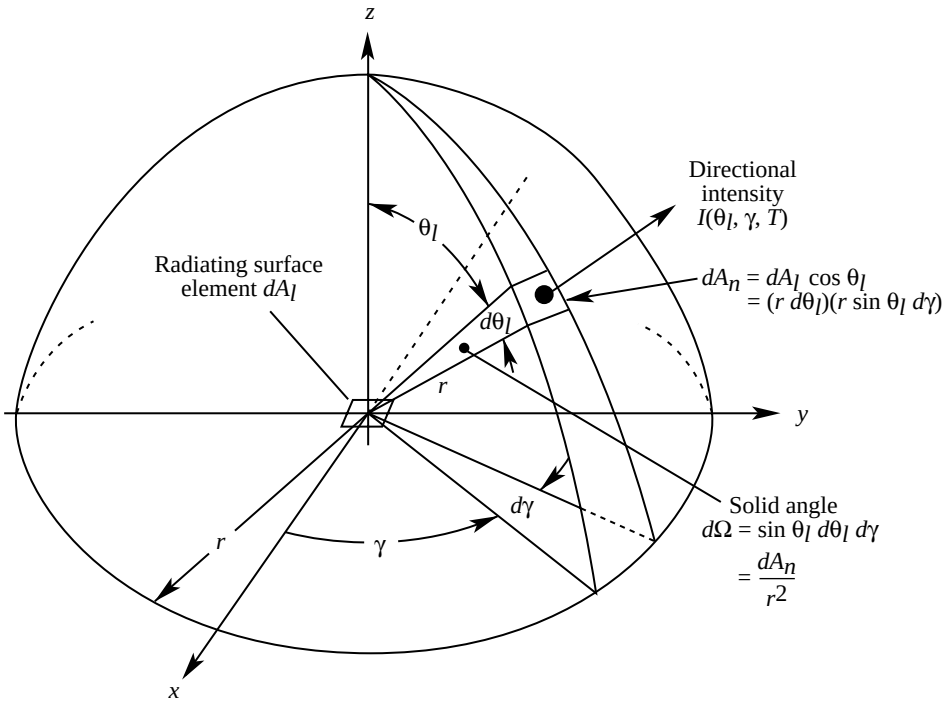

Figure 2. Spherical coordinate system used to define one radiation bundle.

originating at surface l, strikes surface s. In fact, the relative frequency approach gives the probability in the form

$$F_{ls} = \lim_{N_l \to \infty} \frac{N_{ls}}{N_l} \tag{2}$$

The differential view factor between an emitting source element (dA_l) and an element (dA_n) on the hemispherical surface surrounding the source element may be formulated as follows. The geometry and pertinent relations for this development are shown in figure 2.

Writing the spherical surface element heating rate in the form

$$\begin{aligned} dQ'_n &= I_0\, dA_n\, d\Omega \\ &= I_0\, dA_l \cos\, \theta_l \sin\, \theta_l\, d\theta_l\, d\gamma \end{aligned} \tag{3}$$

where I_0 is the diffuse radiation intensity, and noting that the energy radiated by an emitting surface element to all hemispherical space is given by

$$Q'_n = \pi I_0\, dA_l \tag{4}$$

the differential view factor from the emitting element to the element on the hemispherical surface is given by

$$\begin{aligned} F_{ln} &= \lim_{N_l \to \infty} \frac{N_{ln}}{N_l} = \frac{dQ'_n}{Q'_n} \\ &= \frac{\cos\, \theta_l \sin\, \theta_l\, d\theta_l\, d\gamma}{\pi} \end{aligned} \tag{5}$$

In order to obtain a proper probability density function, equation (5) must be normalized by the total view factor to hemispherical space. Obviously, the view factor from dA_l to all hemispherical space, that is, integration of equation (5) over the enclosing hemispherical surface, is unity. Therefore, the expression for the probability density function f_{ln} is equivalent to that given in equation (5). Note that the probability density is a function of the two independent variables, θ_l and γ. Therefore, assuming statistical independence of these random variables, the probability density may be factored into two functions, each involving one variable:

$$\left.\begin{aligned} f_{ln}(\theta_l) &= 2 \cos\, \theta_l \sin\, \theta_l \\ f_{ln}(\gamma) &= \frac{1}{2\pi} \end{aligned}\right\} \tag{6}$$

These marginal probability densities may be related to uniformly distributed functions by defining their

cumulative distributions as follows:

$$\left.\begin{aligned} F_{ln}(\theta_l) &= \int_0^{\theta_l} 2\cos\,\xi\,\sin\,\xi\,d\xi = \sin^2\theta_l \\ F_{ln}(\gamma) &= \int_0^{\gamma} \frac{d\xi}{2\pi} = \frac{\gamma}{2\pi} \end{aligned}\right\} \quad (7)$$

Employing uniformly distributed variables R_{θ_l} and R_γ with range $(0,1)$, values for the random variables, θ_l and γ, can be specified by selection of values for R_{θ_l} and R_γ. Thus, the following relations for determination of θ_l and γ may be written:

$$\left.\begin{aligned} \sin\ \theta_l &= \sqrt{R_{\theta_l}} \\ \gamma &= 2\pi R_\gamma \end{aligned}\right\} \quad (8)$$

These equations allow for random selection of a bundle trajectory from the emission point. The first of these distribution equations governs selection of the angle between the trajectory and the normal to the surface (cone angle). The second relation provides a value for the polar angle measured from a convenient reference (positive x-axis) about the surface normal. Note that these distribution functions apply equally well to diffuse reflection at a surface, where the cone and polar angles are specified relative to the corresponding local coordinate system.

Some of the radiative properties associated with quartz heating systems are rather strong functions of wavelength. Therefore, each bundle must have a wavelength assignment from a representative distribution. A black body at an elevated temperature radiating to space emits radiation with a spectral distribution described by Planck's spectral emissive power law (ref. 26).

$$Q_{\lambda b}(T) = \frac{c_1}{\lambda^5\left(e^{c_2/\lambda T} - 1\right)} \quad (9)$$

where

$$\left.\begin{aligned} c_1 &= 2\pi h c_0^2 \\ c_2 &= h c_0/k \end{aligned}\right\} \quad (10)$$

In these equations, λ is the radiation wavelength, T is the absolute temperature of the radiating body, h is Planck's constant, k is Boltzmann's constant, and c_0 is the speed of light in a vacuum. In order to create a valid probability density function, this spectral emissive power is normalized by the total emissive power, defined by

$$Q_b(T) = \int_0^\infty \frac{c_1}{\lambda^5\left(e^{c_2/\lambda T} - 1\right)}\,d\lambda \quad (11)$$

This integration results in the well-known relation

$$Q_b(T) = \sigma T^4 \quad (12)$$

where σ is the Stefan-Boltzmann constant:

$$\sigma = \frac{2\pi^5 k^4}{15 c_0^2 h^3} \quad (13)$$

Therefore, the proper probability density function has the form

$$f(\lambda, T) = \frac{c_1}{\lambda^5\left(e^{c_2/\lambda T} - 1\right)\sigma T^4} \quad (14)$$

The cumulative distribution function, formulated from this density, is written as

$$F(\lambda, T) = \int_0^\lambda \frac{c_1}{\xi^5\left(e^{c_2/\xi T} - 1\right)\sigma T^4}\,d\xi \quad (15)$$

Hence, a value for the random variable λ is assigned by selection from a uniformly distributed random variable (R_λ) with range $(0,1)$. Unfortunately, the form of the integral in equation (15) is such that it cannot be evaluated in closed form. However, this distribution function is a well-known relation (fractional function of the first kind) and tabulated data of $F(\lambda, T)$ versus λT may be found in many radiative heat transfer texts (e.g., ref. 26; also see table I).

Although the sources in these applications are not in general assumed black, the above discussion is pertinent, since the filaments are assumed gray and the quartz envelopes are assumed diffusely emitting and are assigned a gray body temperature. The reader is reminded that a gray source has the same radiative power spectral distribution as a black source at the same temperature, but the spectral level is lower in magnitude.

Simulation

Each lamp is considered to be composed of two sources, the filament and the quartz envelope (tube). The filament is the primary source, while the quartz envelope is the secondary source, acquiring the bulk of its energy via absorption of energy radiated from

the filament. It is necessary to differentiate between sources, since most systems are sensitive to source size and the distribution of energy between these sources. As a result of the multiple source model, the filament and the quartz envelope interact with each other as well as with the rest of the system. The quartz is treated as a participating medium with specular interfaces and spectral, directional interface properties. However, it is assumed that scattering, birefringence, and polarization associated with the quartz are negligible. All other materials in the system are treated as opaque surfaces. The filament is treated as a diffuse emitter-reflector. Spectral properties of the metallic reflector surfaces are incorporated where available.

With the knowledge of the distribution functions derived in the previous section, an energy bundle history can be constructed. The location for emission from either source (filament or quartz tube) is chosen randomly from two uniform number distributions: one determining the location along the lamp axis (x'-axis, fig. 1) and the other determining the location on the circumference, measured using the positive y-axis as the zero reference direction. The direction of emission (emission trajectory) is then chosen by employing equations (8) to specify the cone and polar angles relative to the local surface coordinate system. Since each source must have a known radiative power, a uniform temperature may be assigned through the use of the equation

$$Q_s = \epsilon \sigma A T_s^4 \tag{16}$$

where Q_s is the source emissive power (discussed in the "Energy Accounting" section), ϵ is the source emissivity, σ is Stefan-Boltzmann's constant, A is the surface area of the source, and T_s is the absolute temperature of the source. This temperature may in turn be used in conjunction with the tabulated fractional function data for equation (15) to construct an interpolation table. Thus, a wavelength is assigned to each bundle through interpolation from this table, based upon the randomly selected value for R_λ.

Quartz envelope. The interaction of radiation with the quartz envelope is somewhat involved. The interfaces between the quartz and the gaseous interior or surroundings are assumed specular. Fused quartz has radiative properties that are highly wavelength dependent for the spectral band of concern (0.2 to 10 μm) (ref. 27). In actuality, the properties are functions of the material index of refraction, which is in turn a strong function of wavelength. Fortunately, much of the needed data exists (ref. 27), but those data are dependent upon the purity of the quartz, which is usually not known for a given lamp. In general, fused quartz is highly transparent to radiation in the range of 0.2 to 2.0 μm, but behaves very erratically between 2.0 and 4.0 μm. Depending upon the purity of the sample, the material exhibits an absorption band originating somewhere in the 2.0- to 4.0-μm range and extending beyond the wavelengths of concern for this application. A fused-quartz sample, representative of that used for the lamp envelopes, was tested for its spectral transmittance in a spectrophotometer. That sample exhibited a rapid drop in transmittance outside the 0.2- to 4.0-μm range. Therefore, the spectral transmittance of the quartz surface was treated as band pass (with a bandwidth of 3.8 μm), which forced treatment of the interface spectral absorptance as band reject. Radiation, within the transmitting band of the quartz, approaching a gas-quartz (from gas to solid) or a quartz-gas (from solid to gas) interface can be either reflected or transmitted. Outside this range, the approximation is made that radiation can only be reflected or absorbed.

The radiative properties of the quartz are also sensitive to direction (angle of incidence). Touloukian and Ho (ref. 27) published spectral reflectance values for several discrete angles for different fused-quartz samples. However, for the present applications, the full range of incidence angle is required (0°–90°). Since the directional, spectral reflectance predicted with Fresnel's equation compared favorably with the available published data, Fresnel's equation was used to determine the directional, spectral reflectivity of the interface. The form of Fresnel's equation used in these applications (ref. 28) is written as

$$\left.\begin{aligned} \rho_n(\theta) &= \frac{a^2 + b^2 - 2a\cos\theta + \cos^2\theta}{a^2 + b^2 + 2a\cos\theta + \cos^2\theta} \\ \rho_p(\theta) &= \rho_n(\theta)\frac{a^2 + b^2 - 2a\sin\theta\ \tan\theta + \sin^2\theta\ \tan^2\theta}{a^2 + b^2 + 2a\sin\theta\ \tan\theta + \sin^2\theta\ \tan^2\theta} \end{aligned}\right\} \tag{17}$$

where

$$\left.\begin{aligned} 2a^2 &= \left[\left(\eta^2 - \kappa^2 - \sin^2\theta\right)^2 + 4\eta^2\kappa^2\right]^{1/2} + \left(\eta^2 - \kappa^2 - \sin^2\theta\right) \\ 2b^2 &= \left[\left(\eta^2 - \kappa^2 - \sin^2\theta\right)^2 + 4\eta^2\kappa^2\right]^{1/2} - \left(\eta^2 - \kappa^2 - \sin^2\theta\right) \end{aligned}\right\} \tag{18}$$

In these equations, θ is the angle of incidence at the interface, and η and κ are the real refractive and absorptive index ratios defined by

$$\left.\begin{aligned}\eta &= \eta_q \\ \kappa &= \kappa_q\end{aligned}\right\} \tag{19}$$

for a gas-quartz interface and

$$\left.\begin{aligned}\eta &= \frac{\eta_q}{\eta_q^2 + \kappa_q^2} \\ \kappa &= \frac{\kappa_q}{\eta_q^2 + \kappa_q^2}\end{aligned}\right\} \tag{20}$$

for a quartz-gas interface. In formulating the index ratio equations, it is assumed that the refractive index of the gas is indistinguishable from that of a vacuum and the absorptive index of the gas is zero (i.e., $\eta_g = 1.0, \kappa_g = 0$). Note that the subscripts q and g refer to quartz and gas, respectively. The complex form of Fresnel's relation is used for these applications, since the quartz exhibits a complex refractive index ($\eta^* = \eta - i\kappa$) in the absorptive regions of the spectrum. Data for the real refractive and absorptive indices of fused quartz were found in reference 27. (See table II.) Supplemental information is attributable to Lang and Wolfe (ref. 29). The two components of reflectivity in equations (17) model polarization effects, which are assumed negligible here. Thus, for unpolarized incident energy,

$$\rho(\theta) = \frac{1}{2}[\rho_n(\theta) + \rho_p(\theta)] \tag{21}$$

Since there is a rapid transition between the transmissive and absorptive regions of spectral quartz properties, it is assumed that the interface is totally reflecting/transmitting within the transmissive band and totally reflecting/absorbing outside of this band. Thus, a value chosen from a new random variable R_ρ (uniform; $0, 1$) can be substituted for evaluating the directional, spectral reflectivity. If R_ρ is less than the reflectivity, the bundle is reflected. Similarly, if the bundle is not reflected, random transmission/absorption tests are conducted.

If the bundle is transmitted, a refracted trajectory is calculated, via Snell's law (ref. 26),

$$\sin^2\phi = \frac{\sin^2\theta}{\eta^2 + \kappa^2} \tag{22}$$

and the subsequent incidence location is determined. In equation (22), ϕ is the refracted angle, and the indices have the same definitions as given previously.

Note that there is a possibility of bulk absorption before the bundle reaches a secondary interface. Bulk absorption is modeled as an exponential decay, controlled by the product of the distance traveled in the quartz and the absorption coefficient. Assuming that the bulk absorption of the medium is uniform (i.e., homogeneous material), the relation is derived subsequently.

The intensity of propagating thermal radiation is constant with distance from the source unless attenuated by a participating medium. The degradation of radiant intensity I of a ray traveling through a medium with absorption coefficient ν is governed by

$$\frac{dI}{I} = -\nu\, ds \tag{23}$$

where s is the distance traveled in the medium (ref. 21). Note that the absorption coefficient is related directly to the absorption index by

$$\nu = \frac{4\pi\kappa}{\lambda} \tag{24}$$

Representing the distance traveled in the quartz, from one interface to another, by Δs, the bulk absorptivity takes the form

$$\alpha = 1 - e^{-\nu\,\Delta s} \tag{25}$$

Upon successfully reaching another interface location (quartz-gas interface), similar requirements exist, including the possibility of total internal reflection.

Metallic reflector. Reflector radiative properties are assumed directionally independent, and spectrally independent where spectral properties are unavailable. Radiative properties of metallic materials are highly surface-condition dependent. Therefore, measurement of the required properties is frequently the only alternative to the simplifying assumptions. Three reflector geometries will be discussed in the "Results and Discussion" section: a flat reflector, a parabolic reflector, and a multilamp curved reflector. Spectral properties were obtained experimentally for a flat titanium reflector, while only estimates of the total values were attainable for the curved, aluminum alloy, commercial reflectors. The spectral reflectivity components of the flat reflector are shown in table III. In all cases, the total reflectivity of the reflector material was taken to be the sum of the diffuse and specular components.

The outcome in the event of reflector incidence is determined by random selection from a uniformly distributed number in the range $(0, 1)$. If the randomly chosen number was less than the combined

reflectivity of the material, the energy bundle was assumed to be reflected. The mode of reflection was chosen by using the relative value of the generated random number as well. That is, if the random number was less than the diffuse reflectivity component, the energy bundle was assumed to be reflected diffusely. If the random number was greater than the diffuse reflectivity component, but less than the combined reflectivity, it was assumed that the energy bundle was reflected specularly. Obviously, if the randomly selected number was greater than the combined reflectivity, the energy bundle was absorbed. This same procedure could have been based upon material absorptivity data just as easily (ref. 13).

System considerations. The position, shape, and three-dimensional extent of all surfaces in the system must be prescribed. Likewise, the trajectory of each energy bundle is prescribed through random selection at all points along the path of the corresponding history. Therefore, determination of whether a particular bundle trajectory will intersect any surface is straightforward using analytic geometry. If the bundle trajectory does not intersect any surface in the enclosure, the energy bundle is "lost" to the surroundings and another bundle is emitted using a new random location on a source. If the bundle is incident upon a surface, the intersection position is calculated and the previous incidence event arguments are employed to calculate a new trajectory. This bundle-incidence location and subsequent fate determination are simulated sequentially until the bundle is either absorbed by a surface or lost from the system.

In most thermal-structure applications, the surfaces involved in the radiant enclosure include the test specimen, source reflectors, and surrounding structure. The effect of the surrounding structure is ignored in this analysis, but may not be negligible for some applications. The source reflectors are generally water cooled (and frequently air cooled as well) to a low temperature in relation to the source and incident surface temperatures. Therefore, emissions from the reflector due to its slightly elevated temperature are considered to be negligible, when compared with the lamps, and only their reflective contributions are considered. Consequently, all energy bundles absorbed by the reflectors are assumed lost from the system. In the examples to be discussed in the results that follow, the test surface is assumed to be perfectly absorbing and nonradiating due to the nature of the experimental procedures that will be used in comparison with the Monte Carlo simulation.

Note that the test specimen may be treated as a participating surface with very little added complexity, as long as it can be represented by a continuous function, thereby conforming to analytic geometry calculations. Also note that specimen participation in a radiant exchange should only tend to increase the mean heating rate and smear local effects of the radiant load. As a result, this analysis is understood to produce a "worst case" distribution and may be augmented in a subsequent thermal analysis of the test surface.

When an energy bundle is incident upon and absorbed by the surface of interest, the "deposition" location is determined and the energy is added to a discrete portion of the surface (bin) containing that location. Energy bundle simulations are executed until a prescribed number of trajectories have been followed to completion, resulting either in energy lost from the system or in energy absorbed by a surface of interest. The resulting distribution of "hits" on the target surface is normalized to give the bivariate relative frequency distribution (i.e., by dividing the number of hits in each bin by the number of bundles used to discretize the reference power). This distribution must be modified further by using the area of the corresponding bins and the radiative power of the source to give the incident radiant heat flux distribution (W/cm^2).

Energy accounting. The radiative power of a single lamp without a reflector, operating in free space, is controlled by the electrical supply and various losses. The losses, even for this most simple case, are very difficult to quantify. Thus, a classical method (refs. 2–4) was employed to attempt indirect determination of an effective lamp power.

The effective radiative power is determined from a single radiative heat flux measurement at a convenient location in the incident plane. This heat flux measurement can be used to infer the radiated lamp power through the use of the equation

$$q(x,y) = \frac{Q_0 H}{2\pi^2 L\alpha}\left(\frac{\beta}{\beta^2+\alpha^2} - \frac{\gamma}{\gamma^2+\alpha^2} + \frac{1}{\alpha}\tan^{-1}\frac{\beta}{\alpha} - \frac{1}{\alpha}\tan^{-1}\frac{\gamma}{\alpha}\right) \quad (26)$$

where

$$\left.\begin{aligned} \alpha &= \sqrt{y^2+H^2} \\ \beta &= x+\frac{L}{2} \\ \gamma &= x-\frac{L}{2} \end{aligned}\right\} \quad (27)$$

That equation is based upon a classical view factor analysis with the corresponding assumptions of a black source and diffuse surfaces (ref. 4). In these equations, $q(x,y)$ is the local radiant heat flux, Q_0 is the radiative (effective) power, H is the vertical distance from the lamp axis to the target plane, L is the lamp lighted length, and x and y are the spatial coordinates in the target plane coinciding with the local heat flux location. It is noted that equation (26) has a slightly different form than that given in references 2–4, which were found to contain an error. The effective radiative power predicted by equation (26) is an overestimate, whereas the effective radiative power predicted by the analogous equations in the previous works was an underestimate. Since the corrected equation, given above, predicted an effective radiative power that exceeded the electrical power applied to the lamp, it was necessary to reexamine the approximations. The cause of this discrepancy is explained subsequently.

The classical method for determining effective lamp power was found to be erroneous because of the nature of the assumptions it employed. That is, since a significant amount of the energy radiated by the filament was virtually unaffected by the quartz tube, the assumption that the quartz tube could be treated as the sole radiator in the classical analysis was in error. The quartz tube diameter was much larger than the tungsten filament, and the radiation source was thus dispersed over a larger area—changing the energy distribution. Furthermore, the tungsten filament was actually a coiled wire that, in conjunction with the quartz envelope as a secondary source, produced a complex radiation energy source and rendered the single effective source approximation ineffective. Since it is known that the unradiated electrical power losses are relatively small, they have been assumed negligible in the subsequent analysis, eliminating the need for an effective power estimate. Consequently, the radiative power of the lamp is assumed equivalent to its supplied electrical power, and the tungsten filament/quartz envelope heat source combination has been modeled. These observations will be supported and discussed in the "Flat Reflector System" portion of the "Results and Discussion" section.

It should be noted further that when multiple lamp systems are modeled as superposed single lamp elements, the real systems they approximate (consisting of multiple sources and/or reflective surfaces) exhibit source augmentation above the individual lamp distributions. Source augmentation is due to shielding from neighboring sources and/or reflections from other surfaces (i.e., the interference between the multiple lamps and between the lamps and the reflector decreases the viewing angle through which radiant energy can escape and thus decreases the amount of radiation lost from the enclosure to the surroundings). When a bundle is absorbed by the filament or quartz in the simulation, it must be reemitted from a new source location selected at random from the corresponding uniform distributions. This process has the effect of increasing the effective power of the sources and redistributing energy amongst the sources. When a bundle is reflected from or transmitted through a source, there is no net effect to the overall energy balance.

A filament has a radiative power governed by the operating electrical power. The surrounding quartz envelope absorbs a percentage of this power through interface and bulk absorption. The presence of reflective surfaces and other sources increases the amount of energy absorbed by all sources. Thus, a coarse approximation of the entire system is required in order to assign a radiative power (and temperature) to the various sources. It should be noted that complicated systems require more refined preliminary simulations in order to converge upon these input parameters. Source temperatures can be calculated from the equation

$$T_s = \left(\frac{n_s}{N} \frac{Q_0}{\epsilon \sigma A_s} \right)^{1/4} \tag{28}$$

where n_s is the number of energy bundles associated with source s (inherent and/or absorbed), N is the total number of bundles inherently available to each filament through discretization of the supplied electrical power, Q_0 is the unaugmented radiative power of a filament (electrical power), and ϵ and A_s are the emissivity and surface area of source s, respectively. Note that Q_0 is related to the source emissive power in equation (16) by

$$Q_s = \frac{n_s}{N} Q_0 \tag{29}$$

Equation (28) applies to filaments and quartz envelopes alike, when used with the appropriate parameter values. Since the system is assumed to be in radiative equilibrium and losses are negligible, the quartz envelopes emit all absorbed energy. The hemispherical emissivity of the fused quartz, as a function of temperature, was estimated from the normal spectral emittance after Touloukian and Ho (ref. 27). These data are tabulated in table III. The tungsten filaments were assigned an emissivity of 0.4 so that their unaugmented temperatures would be consistent with the lamp manufacturer's specifications.

Note that this procedure allows all quantities, such as source temperatures, radiative powers, and resulting radiative heat flux to be normalized by the supplied electrical power of a single filament, and by the number of energy bundles used in discretizing this power.

Computer Implementation

Implementation of the simulation procedure for these applications involves relatively simple logic and programming. Since the spectral content of the radiation from a source is dependent upon source temperature, a means of generating a source spectrum for a given temperature was necessary. Similarly, a logical implementation for the spectral, directional properties and analytic geometry were necessary. In this section, some aspects of these implementations are presented.

Source Spectral Distributions

Since the radiative spectral distribution from a gray body is the same as that of a black body at the same temperature (except reduced proportionally in magnitude), Planck's law may be used to assign wavelengths to the energy emitted by a filament. A quartz envelope has an assigned gray-body temperature from equation (28). Therefore, it has a corresponding Planckian spectral distribution. The tabulated fractional function data discussed in the "Simulation" section are given in table I (ref. 26). The values for the product λT in this table are based upon wavelength in microns and temperature in degrees Rankine. These data are used in an interpolation table that is described subsequently.

The fractional function varies between 0 and 1. Consequently, a value may be selected from a uniformly distributed random variable with range $(0, 1)$, using a pseudo-random number generator (ref. 8), to determine a corresponding λT value. Since the temperature of the source is known, a wavelength is assigned according to Planck's distribution. As a test of this procedure, a simulation of this process alone was executed at two representative source temperatures (2500 K and 833 K), displayed in figure 3. Note the decrement in spectrum amplitude and the shift in the spectral peak to longer wavelengths as the source temperature decreases. The apparent loss in accuracy of the simulated spectra at the longer wavelengths is because relatively few random wavelength assignments fall in that region. This fact is more easily seen by plotting the spectrum corresponding to a 2500-K source with a linear scale (fig. 4).

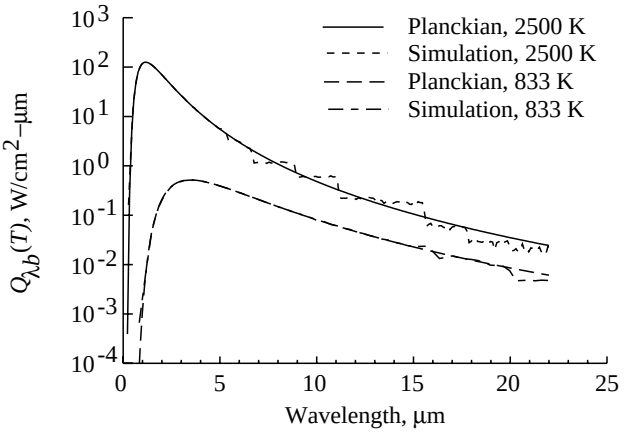

Figure 3. Simulated black-body spectral distributions and corresponding Planckian distributions (2500 K and 833 K) with a sample population of 5×10^6.

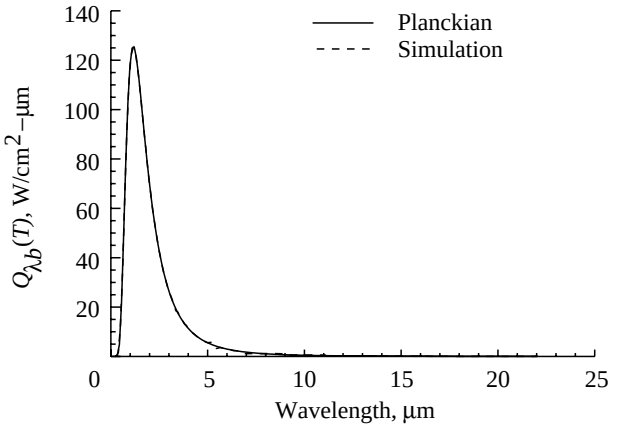

Figure 4. Simulated black-body spectral distribution and corresponding Planckian distribution (2500 K).

Spectral and Directional Properties

The refractive and absorptive indices of fused quartz are wavelength dependent. Representative data for these spectral indices were available from Touloukian and Ho (ref. 27). It is noted that these data for the absorptive index are incomplete in that no data exist below 7 μm. Supplemental information pertaining to the absorptive index is attributable to Lang and Wolfe (ref. 29). This reference suggests that the absorptive index is negligibly small in the spectral region below 7 μm. However, an absorptive index of zero is inappropriate, since that precludes the possibility of bulk absorption (see eq. (25)) and leads to unnecessarily long simulation execution times. Thus, even a very small, but nonzero, absorptive index is crucial. Although actual numerical values for the absorption index in the spectral range below 7 μm are not available from Lang and Wolfe

(ref. 29), data for the absorptive index of window glass, from Hsieh and Su (ref. 30), suggest that a value of 10^{-5} to 10^{-6} may be appropriate. An absorptive index of 5×10^{-6} was used to generate all simulated results presented here. There is also an absence of refractive index data in the wavelength range of 3.7 to 7.0 μm. In this case, supplemental information from Lang and Wolfe (ref. 29) suggests that the available data may be connected with an assumed smooth transitional curve. The resulting curves representing the variation of these indices with radiation wavelength are shown in figure 5.

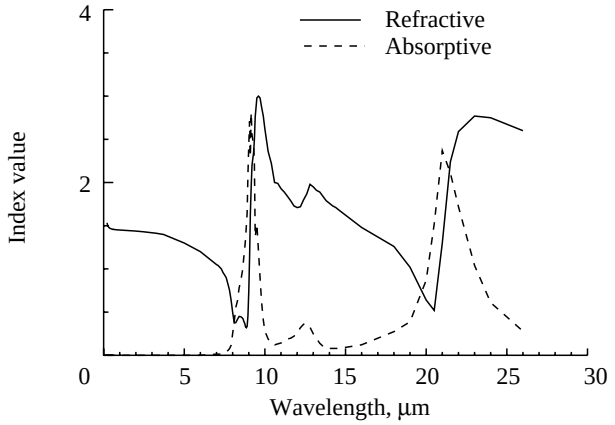

Figure 5. Real refractive and absorptive indices of fused quartz as functions of wavelength (ref. 26).

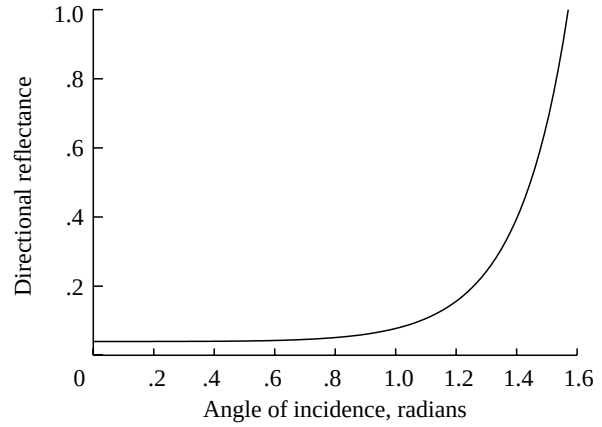

Figure 6. Directional reflectance of a gas-quartz interface ($\eta = 1.5$, $\kappa = 0$).

Since the radiative properties of fused quartz are functions of the refractive and absorptive indices (e.g., Fresnel's eqs. (17) and (18)), they are spectral as well. Fresnel's equations have been used for reproducing portions of the published normal spectral reflectance curves, and they compare well with available empirical data (ref. 27). The radiative properties of fused quartz are also directional. Information pertaining to the directional properties of fused quartz is very sparse and incomplete. However, theoretical directional reflectance values obtained from Fresnel's equations, using the refractive index data just cited, compare favorably with the experimental data that were found (ref. 27). Thus, Fresnel's equations have been used to calculate the directional spectral reflectance of an interface. As mentioned in the "Simulation" section, fused quartz is opaque to radiation with wavelengths greater than about 4 μm. Fused quartz is also opaque to radiation with wavelengths less than about 0.2 μm. Therefore, in these opaque spectral regions the interface transmittance is zero and the directional spectral absorptance of an interface is calculated from

$$\alpha(\theta, \lambda) = 1 - \rho(\theta, \lambda) \tag{30}$$

where θ is the incident angle of radiation at the interface and λ is the radiation wavelength. Similarly, in the transmissive band of fused quartz the interface absorptance is zero and the directional spectral transmittance is calculated from

$$\tau(\theta, \lambda) = 1 - \rho(\theta, \lambda) \tag{31}$$

The directional spectral properties will be presented by separating the effects of each independent variable. Recall that the approximation was made that the reflectance can be used to establish the interface properties in any portion of the spectrum (eqs. (30) and (31)). The directional reflectance for an illustrative situation, where the real refractive index is 1.5 ($\eta = 1.5$) and the absorptive index is 0 ($\kappa = 0$) at a gas-quartz interface, is shown in figure 6. The expected change in the directional reflectance at a quartz-gas interface with the same index values is represented in figure 7. This illustrative situation is characteristic of the transmissive band of the quartz. Thus, the directional absorptance would be zero for all angles of incidence, and the directional transmittance would be the difference between the directional reflectance and unity (see eq. (31)). Note that when the refractive index is entirely real ($\kappa = 0$), the quartz-gas interface exhibits a critical angle of incidence (fig. 7), beyond which total internal reflection occurs. However, with increasing absorption index, the directional reflectance curve flattens and shifts upward, so that critical angle phenomena are lost.

The *normal* spectral properties ($\rho(0, \lambda)$, $\tau(0, \lambda)$, and $\alpha(0, \lambda)$) of a gas-quartz interface are shown in figure 8. Note that for normal incidence, transmission dominates from 0.2 to 4.0 μm. Outside the

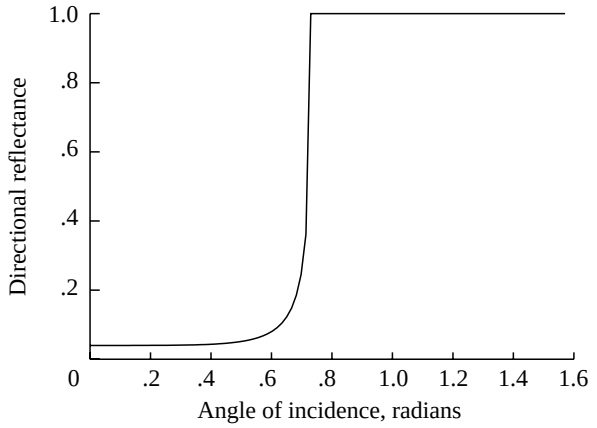

Figure 7. Directional reflectance of a quartz-gas interface ($\eta = 1.5$, $\kappa = 0$).

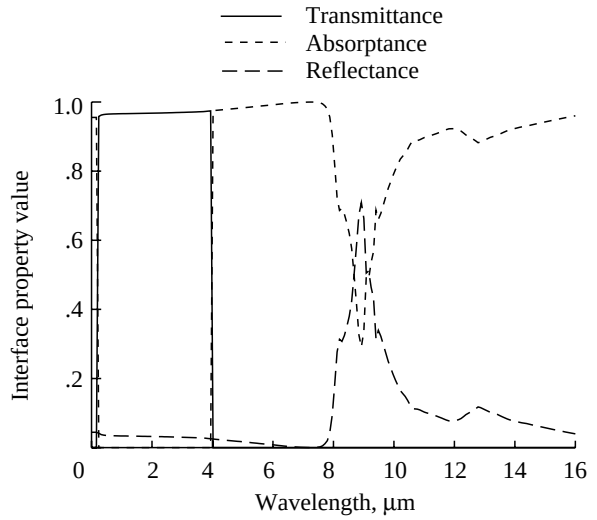

Figure 8. Normal spectral properties of a gas-quartz interface from equations (17)–(21) and (30)–(31).

0.2- to 4.0-μm interval the quartz is primarily absorbing. Also note that the normal spectral properties of a quartz-gas interface are identical to those for the gas-quartz interface, as implied by figures 6 and 7 for an angle of incidence of zero. However, this is not the case for nonzero angles of incidence, as exemplified by figures 9 and 10, which display the spectral properties for an angle of incidence of 70° (1.22 radians) at a gas-quartz and a quartz-gas interface, respectively.

The reflectivity components (specular and diffuse) of a flat, polished titanium reflector were measured for use in the analysis of systems involving flat reflectors. The measurements were made with a sample of the reflector material placed in a spectrophotometer that measured reflectances in the 0.2- to 16.7-μm range. The data used in the simula-

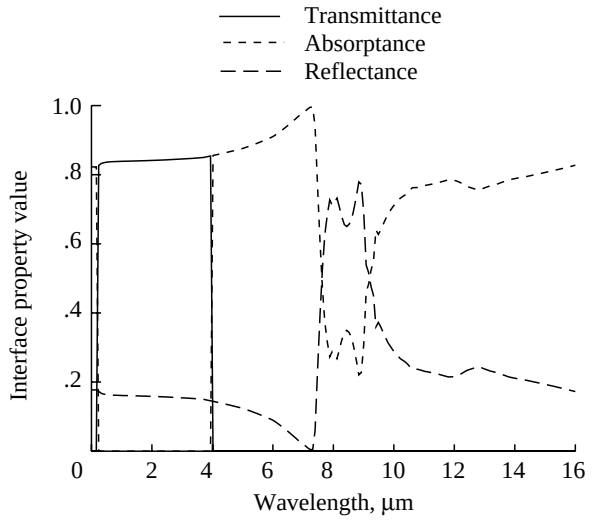

Figure 9. Spectral properties of a gas-quartz interface for an angle of incidence of 70° from equations (17)–(21) and (30)–(31).

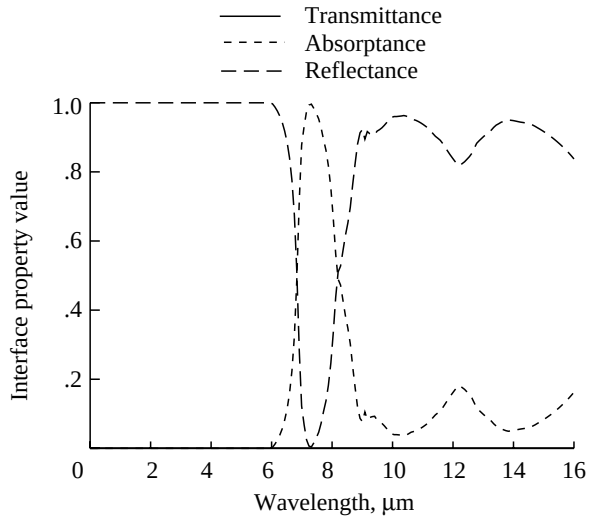

Figure 10. Spectral properties of a quartz-gas interface for an angle of incidence of 70° from equations (17)–(21) and (30)–(31).

tion procedure are presented in figure 11. Recall that the total reflectivity is taken to be the sum of these components. Thus,

$$\rho_t(\lambda) = \rho_s(\lambda) + \rho_d(\lambda) \tag{32}$$

where the subscript t denotes the combined reflectivity.

Analytic Geometry

In order to demonstrate the use of analytic geometry in determining the location of an interaction

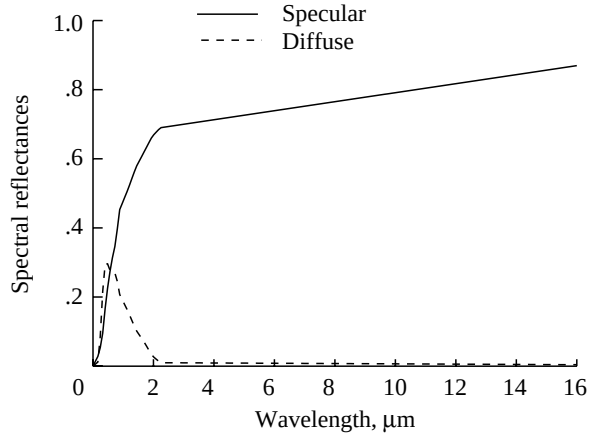

Figure 11. Spectral reflectivity components of a polished titanium reflector.

between an energy bundle and any surface in the system, the governing equations have been formulated for the general case. Consider the bundle position and trajectory to be known in terms of global coordinates (x_0, y_0, and z_0) and direction cosines (a_1, a_2, and a_3). Thus, the bundle trajectory may be written in the parametric, vector form

$$\overline{L} = (x_0 + ra_1)\hat{\imath} + (y_0 + ra_2)\hat{\jmath} + (z_0 + ra_3)\hat{k} \quad (33)$$

where r is the parametric length along the line defined by

$$\frac{x - x_0}{a_1} = \frac{y - y_0}{a_2} = \frac{z - z_0}{a_3} \quad (34)$$

The bundle will be incident upon an arbitrary surface, defined in vector form relative to the global coordinate system by

$$\overline{S} = x\hat{\imath} + y\hat{\jmath} + f(x,y)\hat{k} \quad (35)$$

when the following conditions are true:

$$\left.\begin{aligned} x &= x_0 + ra_1 \\ y &= y_0 + ra_2 \\ f(x,y) &= z_0 + ra_3 \end{aligned}\right\} \quad (36)$$

In equations (36), substitution of the first two equations into the third results in an expression for the determination of r. If the resulting equation has multiple solutions (e.g., several roots of a polynomial), the solutions can be immediately limited to the real roots. From the remaining solutions, only one will be admissible due to physical constraints. When a bundle trajectory is found to intersect with a surface, a random number is generated to test for reflection.

If the subsequent *bundle incidence* event, generated by the random number call, dictates specular reflection, analytic geometry is again employed, in conjunction with Snell's law of reflection, to continue the trajectory. Three vector quantities are needed for this calculation: the trajectory of the incident bundle ($\hat{u}$), the normal to the intersecting surface at the location of incidence ($\hat{n}$), and the normal to the plane containing the two unit vectors ($\overline{N}$). The bundle trajectory is known, and the normal to the intersecting surface is obtained by taking the gradient of the governing surface equation. Of the two possible surface normals, the unit normal is chosen that produces an acute angle between $\hat{u}$ and $\hat{n}$. Subsequently, the final vector quantity is obtained by performing the cross product of the two known vectors. In this manner, three equations for determination of the new trajectory (three unknown new direction cosines) may be formulated as follows:

$$\left.\begin{aligned} \tilde{a}_1^2 + \tilde{a}_2^2 + \tilde{a}_3^2 &= 1 \\ (\tilde{a}_1, \tilde{a}_2, \tilde{a}_3) \cdot \overline{N} &= 0 \\ (\tilde{a}_1, \tilde{a}_2, \tilde{a}_3) \cdot \hat{n} &= \hat{u} \cdot \hat{n} = \cos\theta_i \end{aligned}\right\} \quad (37)$$

where $\tilde{a}_1$, $\tilde{a}_2$, and $\tilde{a}_3$ are the direction cosines of the reflected trajectory and θ_i is the angle of incidence of the bundle. The new direction cosines follow directly from the solution to this set of equations.

If the *bundle incidence* event, generated by the random number call, dictates diffuse reflection, the reflected trajectory is obtained by selecting random cone and polar angles with equations (8). The departing trajectory is defined relative to the local (incident) coordinate system, utilizing the unit normal to the surface at the location of incidence. The new trajectory may be transformed subsequently into global coordinates by using the standard vector (first-order tensor) transformation defined in index notation as

$$u_j = a_{ij} u_i \quad (38)$$

where u_i are the local components of the reflected trajectory, u_j are the global components, and a_{ij} are the direction cosines relating the local and global coordinate axes.

Sample Simulation

The tools and models necessary for numerical simulation of quartz heating systems have been discussed, but the simulation logic is perhaps more clearly presented in the form of a flowchart. Recall that the underlying concept of the simulation procedure is the accumulation of statistical data resulting from a large number of trials (random walks), where

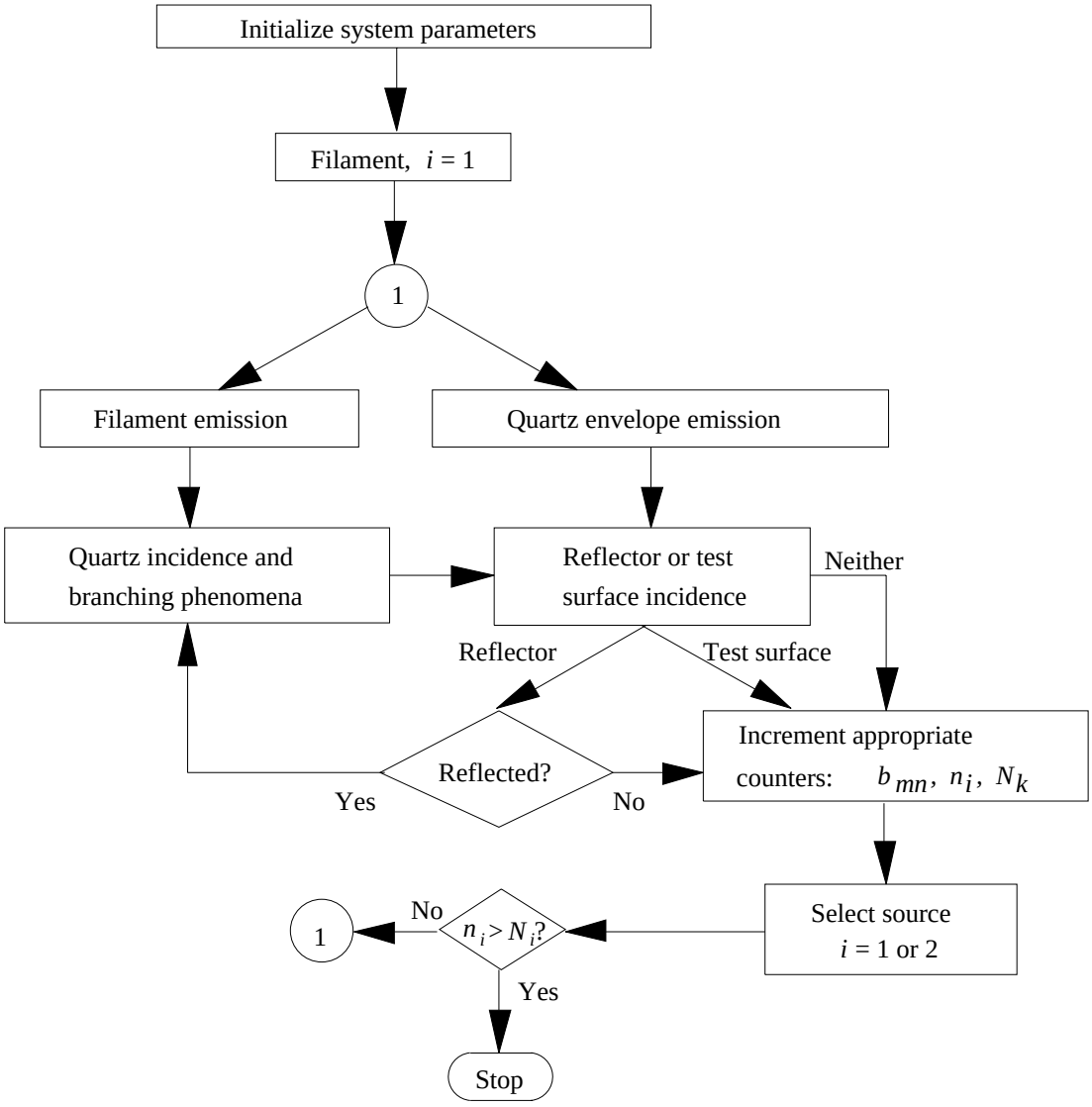

Figure 12. Simulation flowchart corresponding to a system consisting of a single lamp with a flat reflector.

energy bundles are emitted from a source at random and followed subsequently through ensuing trajectories governed by probability distribution functions at each event along their paths. The flowchart shown in figure 12 is a simplified representation of the more detailed version given in the appendix, which corresponds to a representative simulation of a heating system consisting of a single lamp with a flat reflector. The procedure has been summarized below.

Once the system parameters are initialized (e.g., geometry and dimensions, source temperatures and power levels, target surface grid resolution, and common interval limits for random variables), the simulation procedure is initiated from a random location on the filament. Note that the two sources (the filament and the quartz envelope) are simulated concurrently, but the quartz can only emit bundles as it acquires them. Thus, at the start of the simulation, N_1 is some fairly large integer indicative of the filament sample bundle population, and N_2 is zero. Consequently, at marker 1 (fig. 12), for any case other than initiation, the source selector number may equal 1 or 2. Source bundle parameters are then assigned accordingly, at random from the governing probability distributions. These parameters include energy bundle emission location, wavelength, and initial trajectory.

If the filament is the emitter, in a particular bundle *history*, numerous processes can occur within the quartz tube, which may result ultimately in escape to the exterior of the quartz, absorption by the quartz, absorption by the filament, or loss from the system (through the lamp ends). Conversely, when the quartz envelope is the emitter, by definition

the bundle is free to depart from the exterior of the quartz. Either way, once an energy bundle reaches the exterior of the quartz envelope (with a known departure trajectory), a test for incidence on the reflector surface is conducted.

If the energy bundle intersects the reflector surface, a new random number is used to determine whether the bundle trajectory is altered because of reflection or the bundle is lost from the system through absorption. If the bundle is reflected, possible incidence upon the quartz envelope is tested. Incidence requires control to be returned to the multiprocess quartz-interaction module. If the initial bundle trajectory does not intersect the reflector surface, or if a reflected bundle avoids or escapes the lamp, a test is conducted for incidence on the target surface.

For these applications, the target surface is assumed perfectly absorbing. Therefore, any bundle incident upon the test surface is added to the surface bin containing the target surface location (i.e., increment b_{mn}).

Note that if a bundle history is terminated because of absorption by the quartz or the filament, the appropriate sample population counter must be incremented ($N_k = N_k + 1$, where the subscript k denotes the absorbing source number). At the termination of each bundle history, the bundle counter of the initiating source is incremented ($n_i = n_i + 1$, where the subscript i denotes the initiating source). Then an initiating source number is selected at random (1 for filament, 2 for quartz envelope) and control is returned to marker 1. If the particular bundle counter for the chosen source is greater than the corresponding population ($n_i > N_i$), then emission from the other source is attempted (i.e., set $i = 3 - i$). If both bundle counters are greater than their respective populations, the simulation is terminated and the resulting relative frequency distribution over the test surface is normalized to produce the incident heat flux distribution.

A graphical representation of a sample bundle history, applicable to the previous discussion, is shown in figure 13. In this sample, the bundle is emitted by the filament from a randomly selected location (e.g., x_0, y_0, z_0) with a trajectory determined by the direction cosines a_1, a_2, and a_3. The bundle history illustrated proceeds as follows: (1) The bundle is transmitted through the quartz tube. (2) The trajectory is refracted at the gas-quartz interface (inner lamp surface) and again at the quartz-gas interface (outer lamp surface). (3) The bundle trajectory exterior to the quartz envelope intersects the reflector. (4) It is specularly reflected. (The reflected trajectory is described by the direction cosines $\tilde{a}_1$, $\tilde{a}_2$, and $\tilde{a}_3$.) (5) Finally, the reflected bundle trajectory intersects the target surface within the limits of the bin located by the index pair (m, n). Note that at various points along the bundle history, a different event could occur (absorption by the quartz, diffuse reflection by the reflector, etc.). Thus, a different bundle fate can result. With this in mind, it is simple to visualize other possible bundle histories.

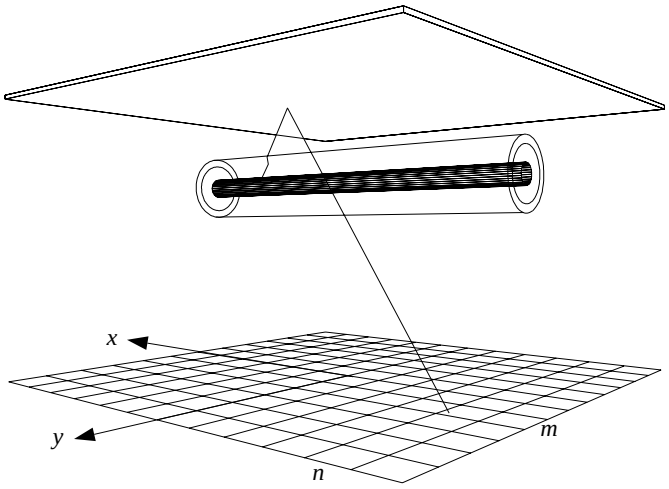

Figure 13. Schematic of flat reflector heating system and example of typical bundle history.

Experimental Methodology

A series of tests were performed in order to investigate the effects of various factors independently and in a simplified manner. The goal of these tests was to provide a means of assessing the validity of the simulation model for use as an analysis and design tool. In all test cases, radiant heat flux measurements were recorded by traversing a Gardon-type heat flux sensor in a test plane along two axes—parallel to the lamp axis (longitudinal, $\pm x$) and perpendicular to the lamp axis, directly below the heater center (transverse, $\pm y$)—as shown in figures 1 and 13.

Experimental Apparatus

An apparatus was constructed for the purpose of measuring the radiant heat flux distribution beneath quartz lamp heating systems of varying complexity. Schematics of the various heating systems are shown in figures 1 and 13–17. Four heating system geometries were studied in order of increasing complexity. These systems can be designated as follows: (1) a single lamp in a free space configuration (no reflector); (2) a single lamp placed below a flat, polished

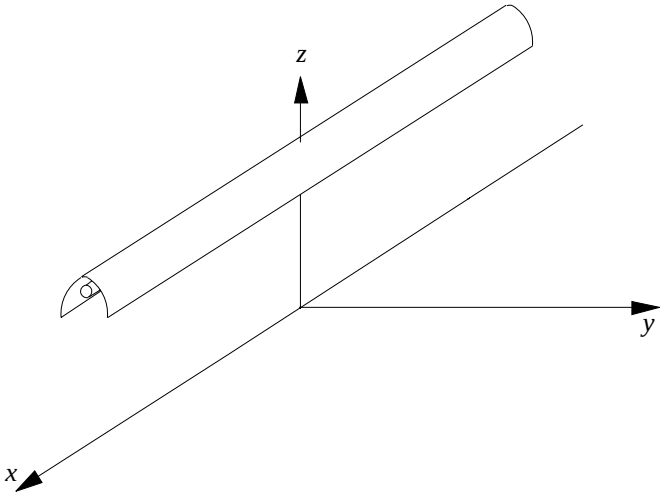

Figure 14. Schematic of parabolic reflector heating system.

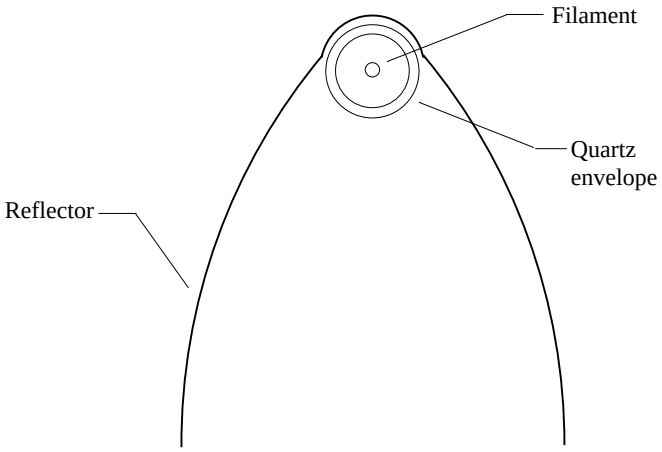

Figure 15. Schematic of single-lamp parabolic reflector unit cross section.

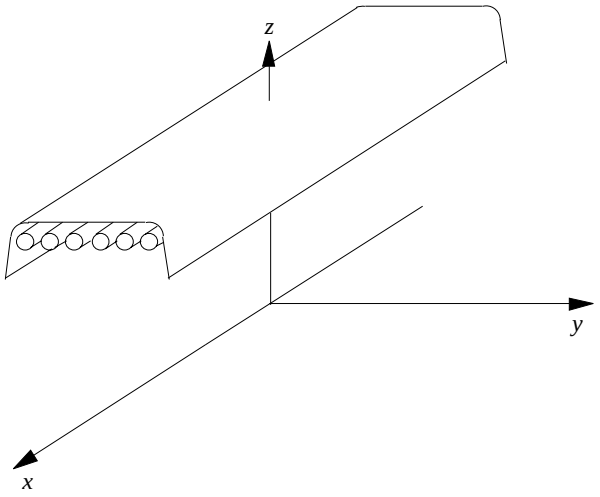

Figure 16. Schematic of multilamp heating system.

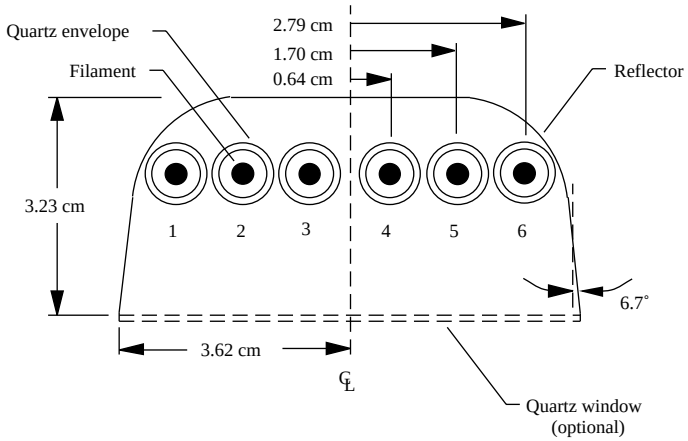

Figure 17. Schematic of multilamp heating system cross section.

titanium reflector; (3) a single lamp placed near the focus of a parabolic aluminum-alloy reflector; and (4) a multilamp system with up to six lamps operated beneath a contoured aluminum-alloy reflector. The geometric detail associated with these systems, which is necessary for the simulation models, is described in the following paragraphs.

A schematic of the single lamp in free space is shown in figure 1. The lamp had a filament lighted length of 25.4 cm and a quartz tube length of 30.48 cm. The filament coil diameter was measured to be 0.14 cm, with quartz tube inside and outside diameters of 0.78 cm and 0.98 cm, respectively.

The flat reflector heating system was constructed by simply placing a flat, polished titanium reflector 3.33 cm above the same lamp (see fig. 13). The reflector dimensions were 25.40 cm by 10.16 cm, with the long dimension of the reflector parallel to the lamp axis. The spectral reflectivity component values for the reflector are given in table III and yield an integrated total reflectivity value of approximately 0.74 ($\rho_s = 0.60$, and $\rho_d = 0.14$).

The parabolic reflector heating system is shown in figure 14. This system consisted of a single lamp with the same filament and quartz envelope diameter dimensions but with a lighted filament length of 63.50 cm and a quartz tube length of 66.04 cm. The lamp axis was located near the focus of a 66.04-cm-long parabolic reflector. The reflector material was an aluminum alloy for which only approximate integrated reflectance components were obtainable ($\rho_s = 0.600$, $\rho_d = 0.245$).

A schematic of the reflector cross section is shown in figure 15. The parabolic contour was idealized for the simulation model by representing the surface by the equation

$$z = z_m - \alpha y^2 \tag{39}$$

where

$$\alpha = \frac{n}{m^2}$$

and n is the height of the parabolic arch at its vertex (2.73 cm) and m is the half-width of the parabola at its base (1.84 cm). The vertex of the parabola is denoted by z_m. It is noted that the section of the parabolic arch that includes the vertex does not exist physically in the actual reflector system, to accommodate the size of the quartz lamp. Thus, the simulation surface geometry excluded this portion of the surface contour and replaced it by the equation for an offset circular arc. The estimated parabola vertex location, the position of intersection of the two curves (denoted by z_s), and an estimated distance from the top of the circular arc to z_s (denoted by h) were used to calculate a radius for the circular section of the reflector. The necessary relation is a mensuration formula, which may be written in the form

$$r = \frac{1}{2}\left(\frac{w^2}{4h} + h\right) \tag{40}$$

where w is the width of the circular section and is found from

$$w = 2\sqrt{\frac{z_m - z_s}{\alpha}} \tag{41}$$

Finally, the center of the circular arc is located with the equation

$$c = z_s - \sqrt{r^2 - \left(\frac{w}{2}\right)^2} \tag{42}$$

Consequently, by estimating the quantities (n, m, z_m, z_s, and h), the entire cross section of this heating system can be defined analytically for a simulation.

The geometry associated with the six-lamp system is analagous to the other units and is shown in figure 16. This multilamp heating system incorporated a water-cooled aluminum reflector with a cross section composed of a flat section with symmetric skirts consisting of a curved section leading to a nearly vertical plane. No reflectance values were obtained for this reflector material, but component values were estimated at $\rho_s = 0.8$ and $\rho_d = 0.1$ in reference 7 from data representative of such materials with similar surface conditions (ref. 31). However, further investigation showed that these values were inaccurate, and a reflectivity of 0.93 ($\rho_s = 0.68$ and $\rho_d = 0.25$) was used for the results shown in this paper. This change is intuitively appealing, since the parabolic and multilamp reflectors are fabricated from the same aluminum alloy, and the physical condition of the multilamp reflector was somewhat better than that of the parabolic reflector. The cross section of this unit, shown schematically in figure 17, was also idealized for the simulation model. The idealized cross section is described below.

The length of the reflector unit was 25.4 cm. The horizontal flat section of the reflector was 3.68 cm wide. The flat inclined sections had a slope of approximately ± 8.5 (or $\pm 6.7°$ from vertical, see fig. 17). For convenience in this discussion, the bottom of these sections will be assigned a z-coordinate of zero. Thus, the points defining the limits of these inclined sections can be defined as follows:

$$\left.\begin{array}{l} y = \pm 3.62 \text{ cm} \\ z = 0.00 \text{ cm} \\ \text{and} \\ y = \pm 3.42 \text{ cm} \\ z = 1.72 \text{ cm} \end{array}\right\} \tag{43}$$

The curved sections were known to be approximately circular and were idealized as circular arcs connecting the flat sections with radius 1.588 cm and center of curvature $y_c = \pm 1.84$ cm, $z_c = 1.64$ cm.

The six lamp locations in this heater were symmetrical about the heater centerline (x-axis) with offsets of ± 0.64 cm, ± 1.70 cm, and ± 2.79 cm, respectively. The lamp axes were approximately 1.14 cm below the flat horizontal section of the reflector. The lamps used in this heating system were a halogen type, with the same quartz tube diameters as the nonhalogen type, but with a filament coil diameter of 0.31 cm. The filament lighted length was 24.77 cm, and the length of the quartz envelope was 25.4 cm.

Because of the high heating levels that can be achieved in the six-lamp system, forced air cooling of the lamps was required. Thus, a 0.15-cm-thick fused-quartz window could be attached to the front of the reflector housing to contain the airflow. A plenum in the back of the reflector housing distributed the air to cool the lamps and their end seals.

A schematic of the entire experimental apparatus is shown in figure 18, where the six-lamp heating unit is shown in a test position. It can be seen that there is a vertical traverse used to adjust the vertical distance between the heating system and the test plane. The requisite system support brackets were interchangeable. One of the supports, used for simulation of a lamp operating in free space, was designed to have minimal participation in the radiant field (reflection, emission). This was accomplished through the following precautionary measures: (1) the support cross-sectional geometry was designed so that

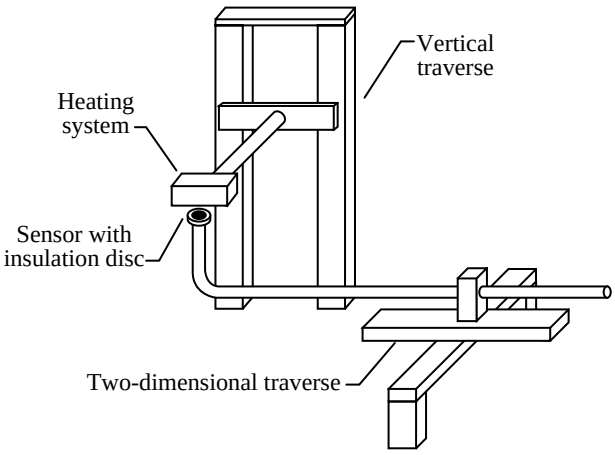

Figure 18. Schematic of experimental apparatus for measurement of radiant heat flux from various heating systems.

the reflective view factor was minimized, (2) the surface was painted with highly absorptive black paint to reduce reflections, and (3) the support was made of high-thermal-conductivity aluminum to reduce the effects of hot spots. The same support bracket was used for the flat-reflector system. The other heating systems were not sensitive to support bracket involvement, since the curved reflector geometries prevented radiation from impinging upon the support bracket.

In an effort to minimize the influence of the surrounding structure on the radiant field, the heat flux sensor was mounted in a steel tube that extended away from a two-dimensional traversing mechanism and toward the heating system, thus placing the sensor in the heated field and preventing any significant interaction with the support. The steel tube also served as a means of routing the sensor cooling lines and electrical lead wires away from the heated area. A thin, washer-shaped insulation disc was mounted concentrically and flush with the upper surface of the heat flux sensor in order to shield the sides of the sensor from quartz-lamp radiation. The traversing mechanism was fabricated by attaching two one-dimensional traversing screws at right angles.

The sensor consisted of a sensing foil, two thermocouple wires, and a water-cooled copper heat sink. Various phenomena affecting the operation of these sensors have been investigated by others (refs. 32 and 33), including heat loss by conduction in the center wire, changes in the heat sink temperature, and changes in the thermal conductivity of the foil. Results shown by Ash and Wright (ref. 33) indicate that changes in the sink temperature and foil conductivity are significant only for transient situations. Since the present applications are limited to steady-state measurements, these effects are neglected. Depression of the foil center temperature due to the presence of the center wire is ignored, since this effect is automatically accounted for by calibration.

The sensor operation utilizes the temperature difference between the sensing foil centerline and its isothermal copper tube base. It is assumed that this temperature difference is governed solely by the incident heat flux. In the present application, heating rates are assumed to be caused by direct radiant heating only. It is also assumed that the temperature gradient through the thickness of the foil is negligible. This assumption is of little consequence, since the foil thickness for these applications is approximately 0.005 cm. The other assumptions are supported by a discussion on the theory of Gardon sensor operation (ref. 8).

Electrical power was supplied to the heating systems from a 480-V substation controlled by a motorized three-phase variable transformer. Since some of the quartz lamp heating systems required air and/or water cooling, an electrical safety interlock was employed, which required proper coolant pressures and flow rates for system operation. A manual override could be employed in situations that did not require the coolant flows.

Experimental Procedures

A series of tests were performed with each lamp type, in the free space configuration, at various specified distances between the lamp and the heat flux sensor. This procedure was utilized to examine the consistency between variations in effective radiative power, predicted by equation (26), with the actual lamp behavior. The effective power was found to increase slightly with increasing lamp-to-sensor distance. This effect was indicative of a reduction in losses with increasing height as well as a reduction in the significance of the sensor dimensions. The changes in effective power with distance from the target surface were not considered significant, since they were of the same order as potential measurement errors in these applications (about 5 percent). Unfortunately, in all cases the effective power predicted by equation (26) was found to be greater than the supplied electrical power. This result was indicative of the classical modeling errors—particularly the radiating quartz surface assumption—discussed in the previous section.

Measurement locations along the two heater axes in the test plane were specified for each experiment based on the predictions from analysis. Consequently, measurements were taken at more closely spaced intervals in areas where the simulation predicted larger gradients. It is noted that the finite size

of the sensing foil placed limits on the measurement resolution and on the interpretation of experimental data in regions of high heat flux gradient.

The heat flux distribution produced by a given heater was determined by traversing the heat flux sensor through prescribed locations along the x and y axes in the target plane. The heating system was shut off between measurements for safety and to prevent excessive heating of the surrounding structure. The heating system was allowed a nominal time of 3 min to reach steady state for each measurement. The transient time was determined experimentally by monitoring the sensor output continuously and noting the time at which the output oscillated about a particular reading for more than about 10 sec. It is interesting to note that this time lapse was fairly standard regardless of the particular heating system being used.

The use of water coolant in the heat flux sensor (which had a mean temperature different from the temperature of the surroundings) induced an apparent heat flux. This effect was easily removed by using an offset feature on the voltmeter employed to measure the heat flux sensor output.

Results and Discussion

Measurements were made of the radiant heat flux produced on a plane by each of four heating systems. As discussed previously, the simulated distributions were normalized by the electrical power supplied to a single lamp in each of the experimental situations. The systems were analyzed in order of increasing complexity in an effort to isolate various complicating effects.

System With No Reflector

The first and most simple system was a single lamp with no reflector. The operating electrical power in this case was 1032 W (i.e., 240 V and 4.3 A), and the distance between the lamp axis and the target plane was 15.24 cm. The experimental and Monte Carlo results from this system are shown in figures 19 and 20. Figure 19 represents the heat flux distribution in the target plane along the x-axis (i.e., directly below and parallel to the lamp axis), while figure 20 shows the heat flux distribution in the target plane along the y-axis. (Refer to fig. 1 for coordinate system.)

It can be seen that the uncorrected simulated results compare well with the experimental measurements of the incident heat flux distribution. Thus, it was concluded that losses associated with a single lamp operating in an unreflected configuration

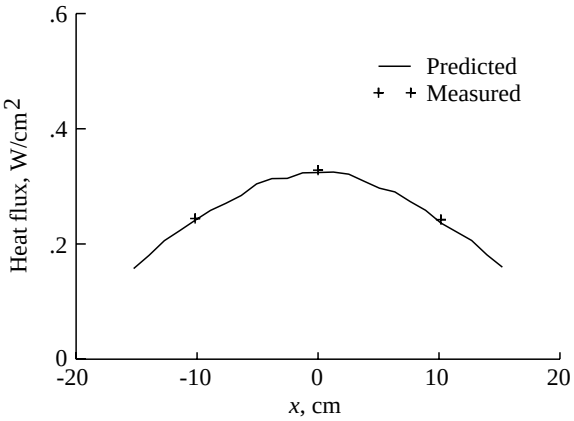

Figure 19. Longitudinal heat flux distribution for single lamp with no reflector (lamp 15.24 cm above target plane operating at 1032 W).

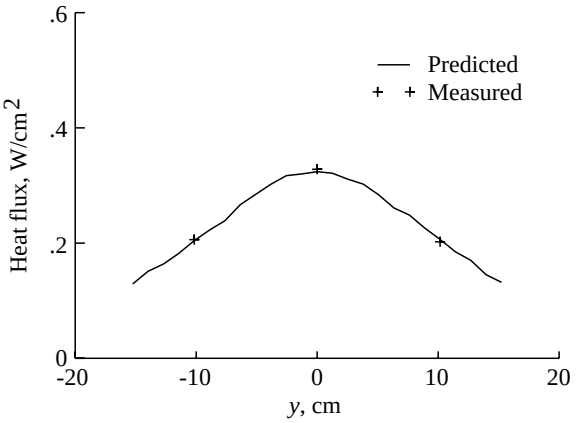

Figure 20. Transverse heat flux distributions for single lamp with no reflector (lamp 15.24 cm above target plane operating at 1032 W).

are very small, and that lamp heating performance need not be adjusted below the supplied electrical power. Note that the simulated heat flux distribution displays irregularities, even though it was generated with a relatively large sample population (10^7). This is indicative of the fact that a majority of the energy bundles do not intersect the test surface. *Importance sampling* techniques (ref. 21) could be used, but the single lamp hardly justified that sophistication. It suffices to say that the addition of a reflector reduces the number of "lost" bundles and therefore improves simulation resolution compared with the bare lamp and the same sample population.

Flat Reflector System

A subsequent test was performed, involving the same lamp, in which the lamp was placed 3.33 cm below a flat, polished titanium reflector and 15.24 cm

above the test plane. The operating electrical power was 1032 W.

It is noted that the flat reflector was not cooled. Therefore, there was some question as to whether it would become a significant heat source because of its elevated temperature. The average steady-state reflector temperature was estimated at 450 K. This estimate was acquired from a finite element thermal analysis of the reflector, based on the analysis discussed in reference 3. A simulated radiant heat flux distribution, resulting from the lamp with no reflector operating at 1032 W and 3.33 cm from a test surface, was used as input. The reflector perimeter was assumed insulated, but the surface was free to exchange heat with the surroundings through both convection and reradiation. From equation (16), the emissive power of the heated reflector at this nominal temperature is approximately 18 W (or 1.7 percent of the lamp power). Consequently, the effect of the reflector emissions was neglected and only lamp-reflected contributions were considered.

The results shown in figures 21 and 22 correspond to the radiant heat flux in the target plane along the x and y axes. The simulated results compare very well with the experimental data, indicating that neglecting the reflector emissions was an acceptable simplification. Note that the heat flux levels in the longitudinal direction (fig. 21) are not very different from the case without a reflector (fig. 19). The cause of this phenomena is more easily seen in figure 22, which shows a rather pronounced dip in the transverse heat flux levels in the target area beneath the lamp. This is indicative of interference between the lamp and the reflector (specular shadowing), which results from the lamp refracting, reflecting, and absorbing reflected energy from the reflector (i.e., energy radiated by the lamp, reflected by the reflector, and incident upon the lamp again). Also note that the addition of a reflector has significantly decreased the number of bundles lost from the system, as is evident by the increase in the mean heat flux.

Five simplified versions of the simulation model for the flat reflector system were created to investigate the effects of a variety of modeling issues. These simplifications were implemented independently and included (1) treating the lamp as a diffusely radiating (gray) filament (ignoring all effects of the quartz), (2) considering the quartz envelope to be a diffusely radiating (black) source, (3) assuming reflected contributions to be totally diffuse, (4) neglecting the absorptive properties of the quartz, and (5) assuming the energy absorbed by the quartz to be lost. The results of this study are shown in figures 23—26.

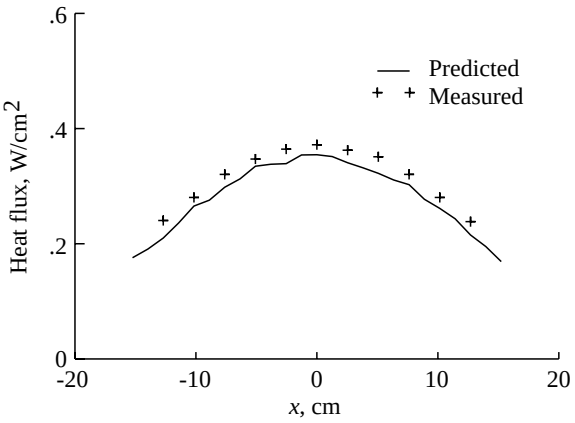

Figure 21. Longitudinal heat flux distribution for single lamp and flat reflector (lamp 15.24 cm above target plane operating at 1032 W).

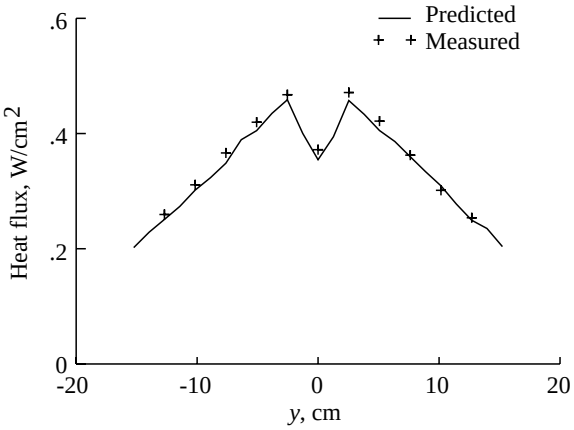

Figure 22. Transverse heat flux distribution for single lamp and flat reflector (lamp 15.24 cm above target plane operating at 1032 W).

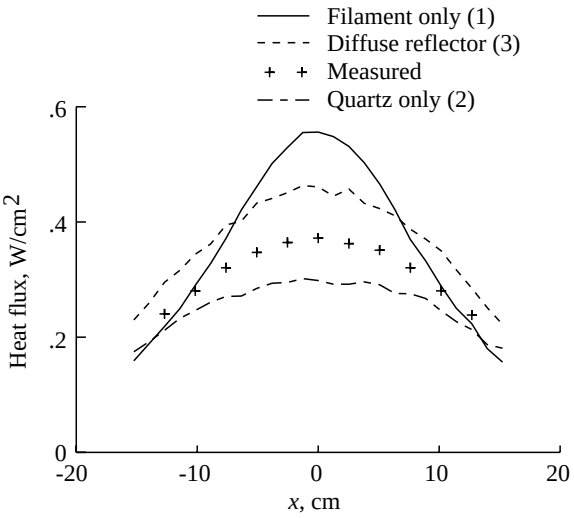

Figure 23. Longitudinal heat flux distribution from three simplified models of flat reflector system.

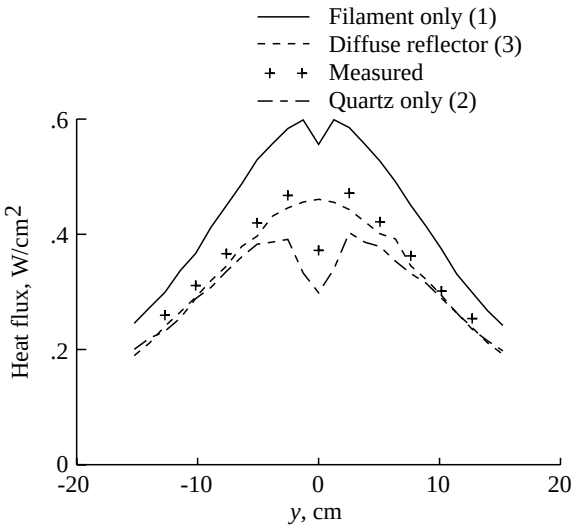

Figure 24. Transverse heat flux distribution from three simplified models of flat reflector system.

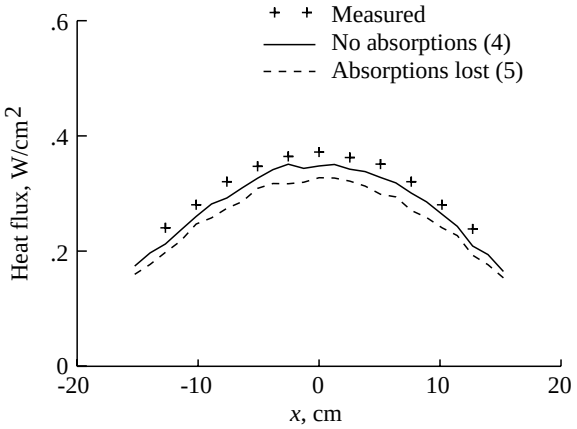

Figure 25. Longitudinal heat flux distribution from two simplified models of flat reflector system.

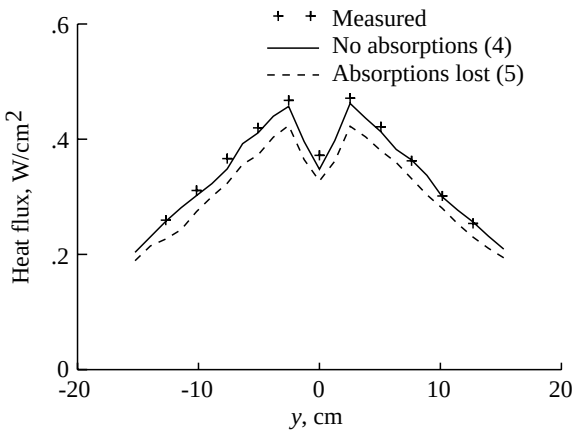

Figure 26. Transverse heat flux distribution from two simplified models of flat reflector system.

It can be seen in figures 23 and 24 that when the effects of the quartz envelope are ignored, the lamp-reflector interactions are much less significant, resulting in higher heat flux levels and a less significant interference dip in the transverse distribution. This model approximates the lamp as a line source. Conversely, when the quartz envelope is treated as the sole diffuse emitter, the effect of lamp-reflector interference is accentuated because radiation is not allowed to pass through the quartz. This model is the statistical equivalent of the classical equation (26). Note that in order to match the experimental results, the entire distribution corresponding to this case requires scaling by a greater lamp power than actually supplied, exemplifying the modeling error discussed previously. Thus, these two simplified models indicate that the filament and the quartz envelope must both be modeled to produce consistent simulations. It can also be seen that treating the reflections as totally diffuse is not an accurate model, since this treatment of the reflected contributions tends to smear any interference effects (as seen most clearly in the transverse test results). Because this system is only moderately sensitive to these modeling issues, due to the weak interaction between the lamp and the reflector, these model refinements are considered critical for simulation of more complex systems. Note that in this case, and in all the cases to be discussed, the transverse heat flux results are the most sensitive, for correlation purposes, because of geometry and interference factors.

In figures 25 and 26, it can be seen that the model that neglects the absorptive properties of the quartz (i.e., the quartz is only refractive) produces results nearly identical to the full model used to generate the simulated distributions in figures 21 and 22. This is attributable to the fact that the lamp filament temperature for this case was estimated at 2555 K. As shown in figure 4, the spectral peak of the energy radiated by the filament is approximately 1 μm, and a small percentage of the total energy lies in the spectral region beyond 4 μm. Therefore, it can be seen that this simplified model is very similar to the full model, and the refractive properties of the quartz produce the most important alteration to the heat flux distribution. Finally, if the absorptive properties of the quartz are modeled, but the absorbed energy is assumed lost, the resulting heat flux distribution is significantly lower in magnitude. This result shows that a significant amount of energy is indeed absorbed by the quartz (with a transmissive band upper limit of 4 μm), which further supports the observation that the refractive effects of the quartz are dominant.

Parabolic Reflector

Experimental radiant heat flux measurements were also obtained from the parabolic reflector heating system. The lamp axis was set at approximately 30.48 cm above the target plane. Thus, values for z_m and z_s were estimated at 30.87 cm and 30.70 cm, respectively. The geometric model and other pertinent dimensions were discussed in the "Experimental Apparatus" section. The measured electrical input was 2754 W. The experimental measurements are included in figures 27 and 28, in comparison with the Monte Carlo simulation. Since the dimensions associated with the reflector cross section are rather small, and the reflector has a focal point, this system is very sensitive to parameters such as lamp placement, reflector geometry, and reflector reflectivity components. Thus, close correlation with experimental results for this system is considered to be relatively difficult. However, good results were obtained, as can be seen in the comparisons.

It is noted that the use of the estimated reflectivity components ($\rho_s = 0.6$ and $\rho_d = 0.245$) produced inaccurate results in that the simulated transverse distribution exhibited a much higher peak flux and a narrower high-intensity heat flux distribution interval (fig. 28). It can be seen that the area under the simulated curve is approximately the same as that under a curve drawn through the experimental data. Therefore, a parametric study of the specular and diffuse reflectivities was conducted to determine possible causes for the shape discrepancy. This parametric study showed that the reflectivity components could be adjusted to values of $\rho_s = 0.4$ and $\rho_d = 0.425$ to achieve the improved heat flux contour shapes shown in figures 27 and 28. Our parametric studies also investigated shifts in the upper limit of quartz transmittance to test for possible quartz purity deficiencies and scattering effects. It was found that changes in that parameter, over physically acceptable limits, did not improve simulations. Thus, it was concluded that errors in the model geometry were the primary cause of the discrepancies between the experiment and its simulation. This observation is supported by the observable discrepancies in the improved transverse results (fig. 28). Note that the areas under the respective distributions are no longer equal, which is evidence of energy leakage (energy escaping the limits of the test area due to the high diffuse reflectivity component). Also note that systems with predominantly specular reflectors are naturally more sensitive to reflector contour slope inaccuracies. Therefore, it was concluded that the actual reflectivity components are modeled more correctly by the original estimates (predominantly specular), but inaccuracies in the geometric model of the reflector contour distributed the reflected energy somewhat differently from the actual manufactured reflector geometry.

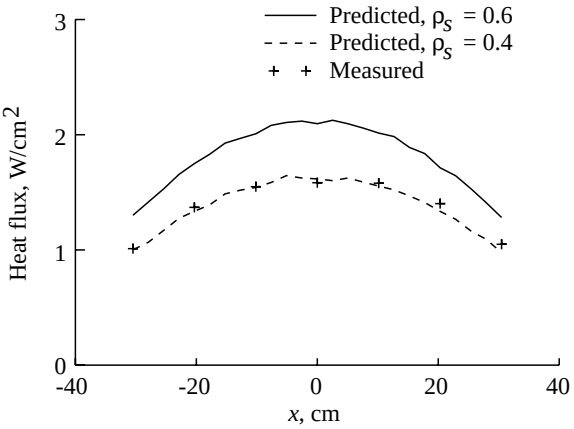

Figure 27. Longitudinal heat flux distribution for single lamp and parabolic reflector (lamp 30.48 cm above target plane operating at 2574 W).

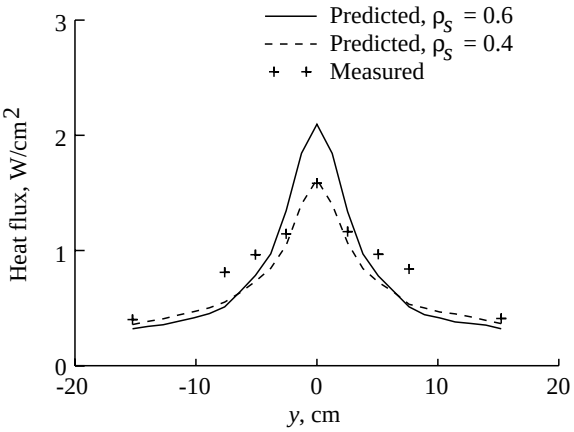

Figure 28. Transverse heat flux distribution for single lamp and parabolic reflector (lamp 30.48 cm above target plane operating at 2574 W).

Multilamp System

A simulation model was also developed for analysis of the six-lamp, contoured reflector heating system represented schematically in figure 17. The heating system was positioned such that the lamp axes were 15.24 cm above the test plane. Air cooling of the quartz envelopes is recommended in the multilamp unit, even at reduced operating conditions. Since it is desirable to isolate the complicating factors associated with the airflow and the quartz window, which is required to contain the flow, all the tests involving this unit were performed at 120 V (one-fourth of the rated voltage), which corresponds to an

individual lamp power of 744 W. This enabled isolation of the quartz window and air-cooling effects by allowing tests to be performed as follows: (1) with the window removed and no air cooling, (2) with the window in place but no airflow, and (3) both with the window in place and with air cooling. This conservative (low power) operating condition is thought to be of little consequence in establishing lamp system performance, since the basic characteristics of the heating system are not affected by the operating power, except for the obvious increase in source radiation levels and shifts in source spectra to shorter wavelengths with increasing input power. All the reported radiant heat flux distributions that follow resulted from experiment and/or simulation of the multilamp unit with one or more lamps in operation.

The results shown in figures 29 and 30 correspond to heat flux distributions along the x and y axes in the target plane, produced by a single lamp placed in the positive outermost position (+2.79 cm). It is noted that some discrepancies in this comparison are attributable to geometrical inaccuracies of the simulation model. Recall that the simulation model assumes that the curved sections of the reflector contour are perfectly circular. The proximity of the lamp to the curved reflector surface in the extreme, +2.79-cm location sensitizes the system to such geometric inaccuracies. This observation is supported by the jagged dip in the simulated distribution at approximately $y = -9$ cm. In viewing the simulated system geometry, drawn to scale, it was determined that the dip in the simulated distribution corresponds to lamp shadowing in the focused radiation streaming from the circular reflector section.

Similarly, results shown in figures 31 and 32 represent the longitudinal and transverse heat flux distributions generated by a single lamp placed in the +1.70-cm location. The distributions in figures 33 and 34 resulted from a single lamp operated in the +0.64-cm location of the multilamp unit. Note that the agreement between simulation and experiment improves as the lamp location progresses toward the center of the reflector unit. This further supports the contention that inaccuracies in the model of the experimental heating unit geometry (e.g., the actual system has slightly noncircular curved sections) cause discrepancies, since the effect of these geometric anomalies decreases with increasing distance between the lamp and these reflector sections (i.e., as the lamp location progresses toward the symmetry plane). Thus, it is concluded that systems involving curved reflectors are very sensitive to discrepancies between the actual geometry and the simulated

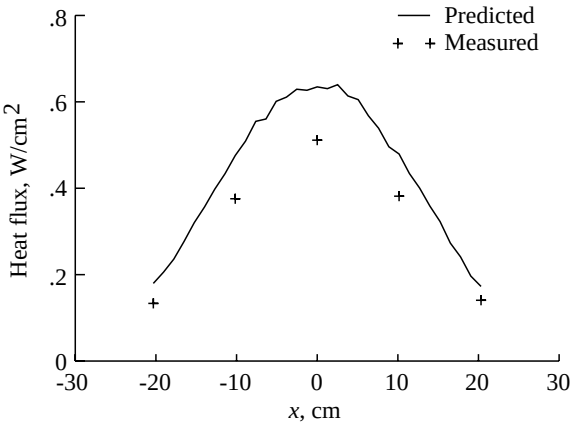

Figure 29. Longitudinal heat flux distribution from one lamp placed at 2.79-cm position (see fig. 17) in multilamp heating system (lamp 15.24 cm above target plane operating at 744 W).

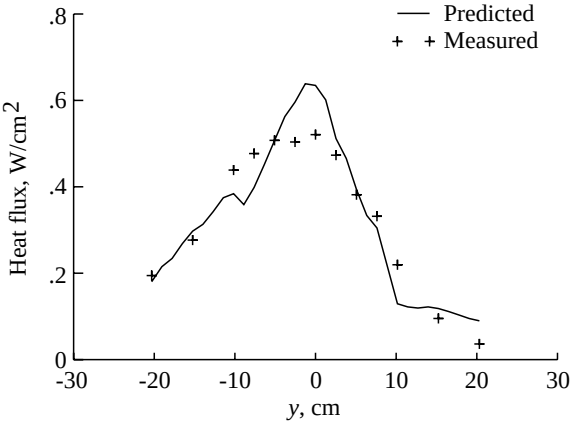

Figure 30. Transverse heat flux distribution from one lamp placed at 2.79-cm position (see fig. 17) in multilamp heating system (lamp 15.24 cm above target plane operating at 744 W).

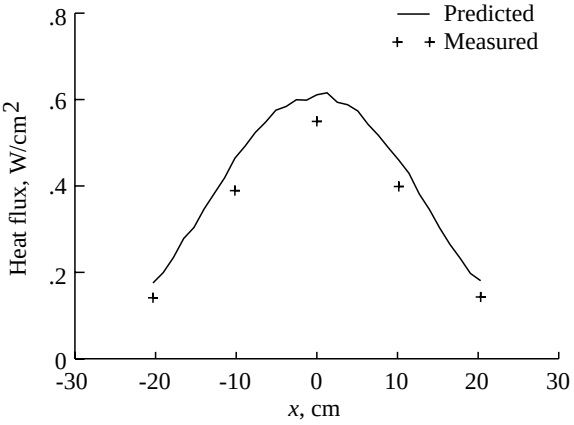

Figure 31. Longitudinal heat flux distribution from one lamp placed at 1.70-cm position (see fig. 17) in multilamp heating system (lamp 15.24 cm above target plane operating at 744 W).

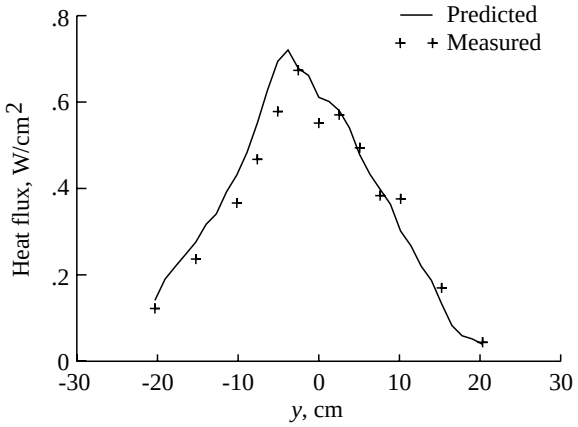

Figure 32. Transverse heat flux distribution from one lamp placed at 1.70-cm position (see fig. 17) in multilamp heating system (lamp 15.24 cm above target plane operating at 744 W).

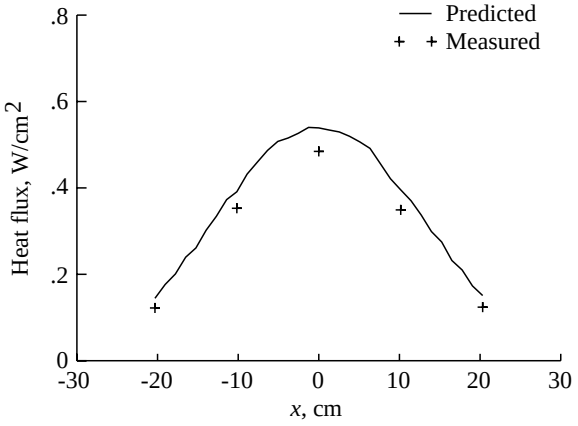

Figure 33. Longitudinal heat flux distribution from one lamp placed at 0.64-cm position (see fig. 17) in multilamp heating system (lamp 15.24 cm above target plane operating at 744 W).

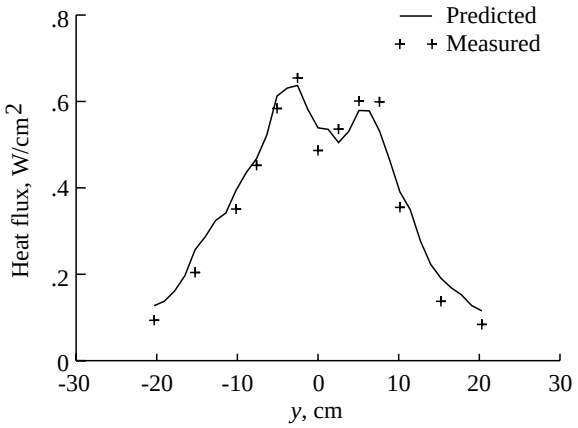

Figure 34. Transverse heat flux distribution from one lamp placed at 0.64-cm position (see fig. 17) in multilamp heating system (lamp 15.24 cm above target plane operating at 744 W).

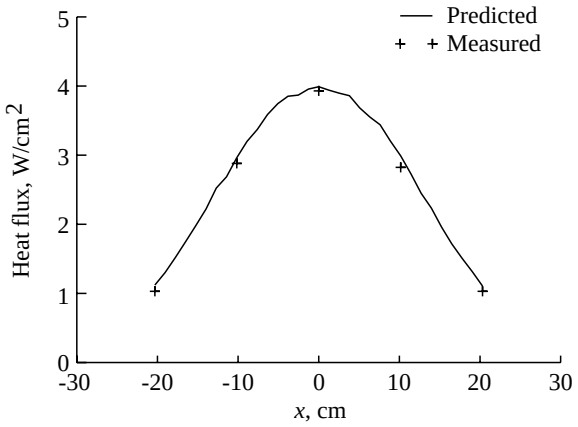

Figure 35. Measured and simulated longitudinal heat flux distributions from a fully operational six-lamp unit without quartz window or air cooling (lamps 15.24 cm above target plane operating at 744 W).

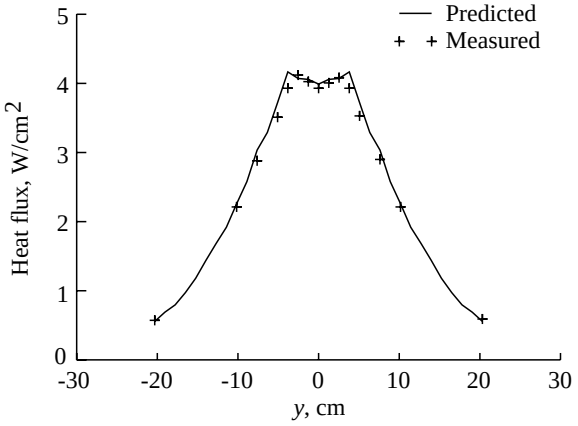

Figure 36. Measured and simulated transverse heat flux distributions from a fully operational six-lamp unit without quartz window or air cooling (lamps 15.24 cm above target plane operating at 744 W).

geometry, especially when the characteristic lamp-reflector distance approaches the lamp diameter.

The radiant heat flux distributions shown in figures 35 and 36 are representative of those produced by the multilamp unit with all six lamps installed and in operation. It is interesting that very good results were obtained for this most complicated case. However, it is not surprising, since the superposition of the distributions from many independent sources tends to smear the individual lamp effects. Furthermore, the interactions between the many sources in the actual six-lamp case alter the distribution of radiant heat flux further.

In order to quantify the effect of the multilamp interactions, the empirical distributions from symmetrically placed lamps were superimposed (e.g., lamps 1 and 6 in fig. 17) to produce three sets of symmetric two-lamp longitudinal and transverse distributions. The three resulting data sets for each direction were superimposed to give pseudo six-lamp distributions. This procedure was also performed with the simulated distributions for the single-lamp cases to produce simulated pseudo six-lamp distributions. These distributions are compared with the actual six-lamp distributions in figures 37 and 38. The empirical and simulated superposition distributions compare fairly well. However, the superposition distributions are significantly lower in magnitude than the actual six-lamp distributions. This fact can be explained through geometric arguments described in the following paragraphs.

If only the lamp located at +2.79 cm is present in the heater (see fig. 17), a large percentage of the radiation incident upon the reflector is lost to the surroundings (e.g., initial bundle trajectory striking the horizontal flat reflector section with a subsequent specularly reflected trajectory leaving the reflector contour and escaping the target area). However, if other lamps are present to intercept this radiation, much more of the total energy available will be confined within the limits of the target area. It is apparent that the more lamps there are, the greater the lamp enhancement and the larger the difference between the actual multilamp distributions and the single-lamp superposition distributions.

In order to test this observation, an experiment was conducted to quantify this effect. Starting with a single lamp in the +2.79-cm position, five measurements of the radiant heat flux were obtained at the central location ($x = 0$, $y = 0$) in the test plane (15.24 cm below the lamp axes) while incrementing the number of adjacent lamps in succession from two to six lamps. The lamp enhancement factor was calculated by determining the relative difference between these measurements and their empirical superposition analogs. The results of this procedure are shown in figure 39. Note that, as expected, the enhancement factor increases with the number of lamps present in the heating system. It can also be seen that increases in the enhancement factor are less significant with the addition of the more remote lamps (lamps 4, 5, and 6), since the interaction with these lamps is more moderate.

Additional experiments were conducted to attempt quantification of the quartz window and air-cooling effects. One concern was that there would

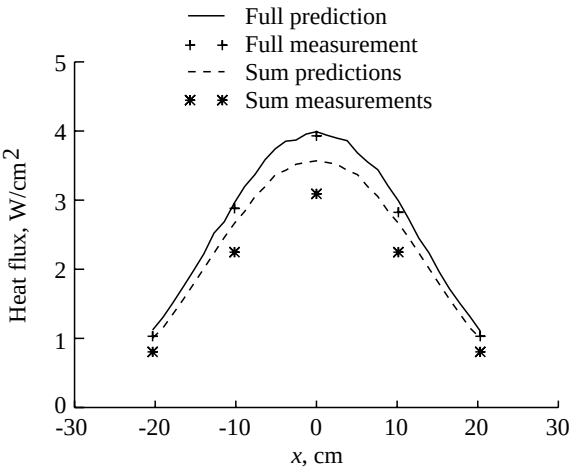

Figure 37. Superposition of longitudinal single-lamp results (experimental and simulated) and six-lamp experimental and simulated distributions.

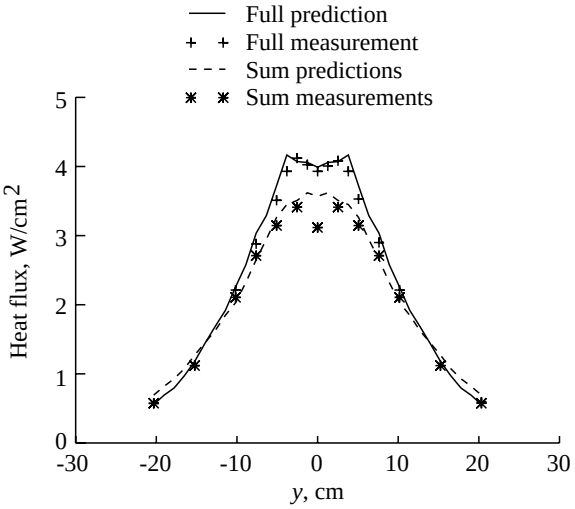

Figure 38. Superposition of transverse single-lamp results (experimental and simulated) and six-lamp experimental and simulated distributions.

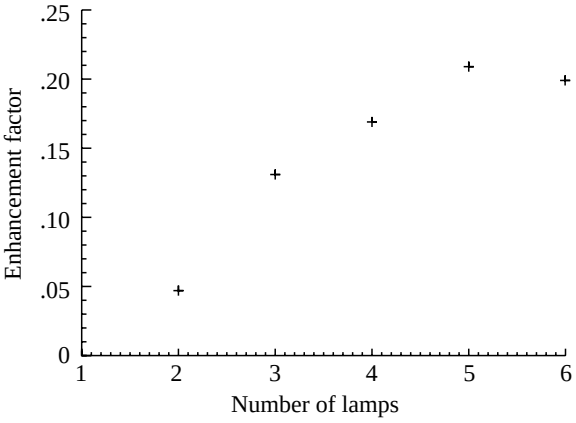

Figure 39. Enhancement factor as a function of number of lamps in multilamp system.

be a change in the shape of the distribution (loss of symmetry in the longitudinal direction) due to the airflow, since the air temperature could increase significantly and lose cooling efficiency as it passed along the lamp length. This effect was tested by recording measurements in the target plane at locations on the x-axis symmetrically located about the heating unit center. Within the inherent accuracy of these experiments, this effect was not detectable. Therefore, it was assumed that the distributions were not altered in any significant manner, and that the accuracy of the corresponding simulation models could be assessed by comparing experimental and simulated heat flux values at a single location (central location).

Measurements of the radiant heat flux at the central location in the test plane were recorded with one lamp and with six lamps in the multilamp heating unit, with the quartz window in place without air cooling and with the quartz window in place with air cooling. Differences between the measured values and the simulated results are most discernible for all six lamps operating in the multilamp heating unit. As figures 40—43 show, the window reduced the central heat flux level by about 7 percent and the air cooling reduced the level by an additional 18 percent, requiring simulation corrections for both effects. The simulation modifications are described subsequently.

The simulation model was altered for inclusion of the quartz window by simply adding a quartz plate module to the program logic such that any bundles escaping the reflector unit intersected the glass plate. Bundles in this category were subjected to interface reflection, transmission, and absorption, and bulk absorption treatments similar to the quartz envelope interactions. The bundles absorbed by the window were then radiated toward the test surface from positions picked (uniformly) at random on the lower surface of the window (i.e., the window was treated as an isothermal radiator). The heat flux distributions (longitudinal and transverse) predicted by the modified simulation are shown in figures 40 and 41, along with the corresponding measured center point heat flux.

The power lost to the air was experimentally determined by measuring the heater air inlet temperature, the exhaust temperature, and the mass flow rate (18.3°C, 45°C, and 0.034 kg/s, respectively) from the multilamp unit with six lamps installed. Dividing this power by the number of lamps (six) resulted in an estimated loss of 151 W per lamp (20 percent of the applied power). The simulation was then

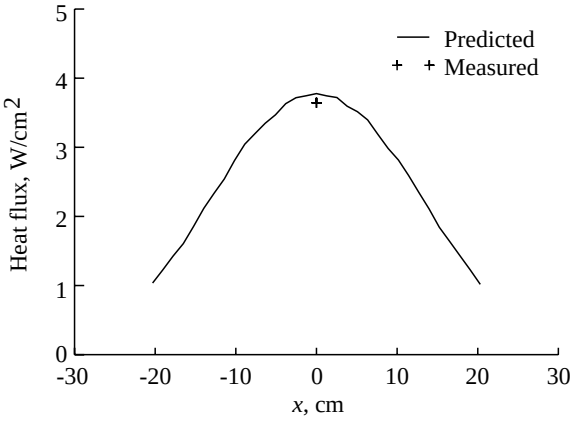

Figure 40. Simulated longitudinal distribution and measured heat flux at central location 15.24 cm beneath multilamp unit with six lamps (each operating at 744 W) behind a quartz window.

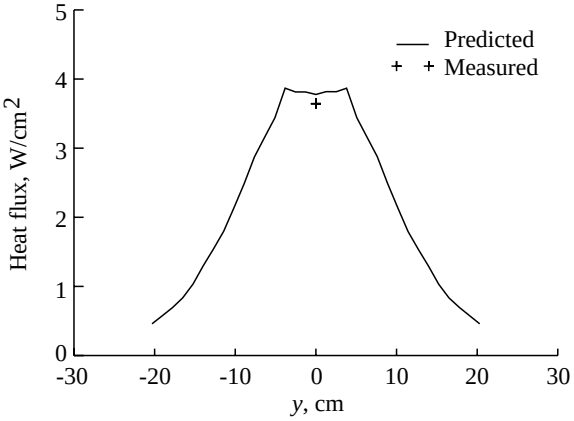

Figure 41. Simulated transverse distribution and measured heat flux at central location 15.24 cm beneath multilamp unit with six lamps (each operating at 744 W) behind a quartz window.

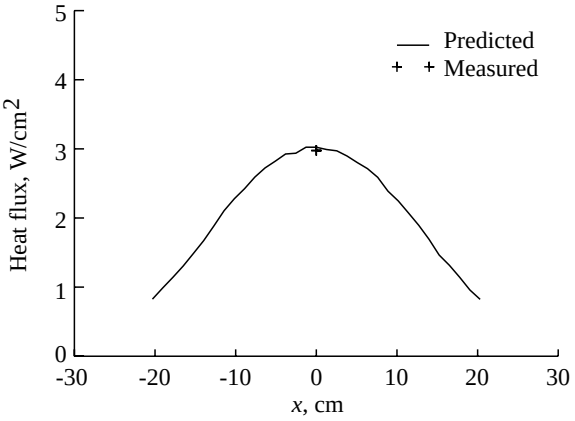

Figure 42. Simulated longitudinal distribution and measured heat flux at central location 15.24 cm beneath multilamp unit with six lamps (each operating at 744 W), quartz window, and forced air cooling.

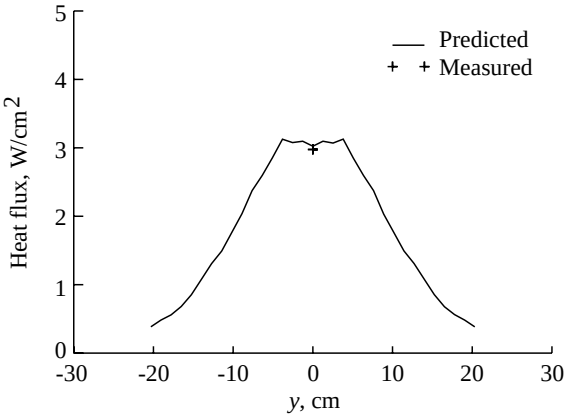

Figure 43. Simulated transverse distribution and measured heat flux at central location 15.24 cm beneath multilamp unit with six lamps (each operating at 744 W), quartz window, and forced air cooling.

altered to discard the number of bundles from each quartz envelope corresponding to the percentage reduction in available power, which was lost to the air. The percentage was established by dividing the 151-W loss by the power predicted by equation (16) for each envelope. It is noted that the fused-quartz window also contributed to the power lost to the air. However, a flow analysis to determine the various losses at that level of detail could not be justified, nor was it considered to be necessary, as can be seen by the close agreement with experiment, shown in figures 42 and 43.

Concluding Remarks

A method has been developed for predicting the radiant heat flux distribution from heating systems consisting of tungsten-filament tubular quartz lamps with and without reflectors. The method is an application of Monte Carlo simulation and allows for a multitude of model refinements not amenable to a classical analysis. Some examples of higher order effects easily included in the numerical procedure were treatment of spectral and directional properties, analysis of specular reflection from curved surfaces, and analysis of radiant transfer through participating media. The simulation model of the basic components of a quartz heating system permit the following conclusions.

The tungsten filament and the fused-quartz envelope of a quartz lamp unit should be modeled separately and allowed to interact. The filament is the primary source, while the quartz tube participates by reflecting, refracting, and absorbing energy and is a secondary source, acquiring a majority of its energy through absorption of energy radiated by the filament. The filament could be treated as an opaque, gray emitter-absorber, while it was necessary to model the quartz envelope as a participating (absorbing) medium between two specular interfaces that were partially reflecting, transmitting, and absorbing. Polarization and scattering due to the quartz could be neglected. Reflectors were modeled as opaque surfaces and the reflectivity was modeled effectively as a combination of specular and diffuse components.

The radiative power of each filament was modeled successfully as a random population of photon bundles of equal energy, distributed over a temperature-controlled wavelength spectrum. Temperatures could be assigned to the sources by using a simple relation involving the ratio of the total number of energy bundles emitted by each source to the standard sample population of a filament, the radiative power of a filament, and the respective source emissivities and areas. Given the calculated source temperatures, wavelengths could be assigned to bundles emitted by the sources according to Planck's law. All the necessary probability distribution functions could be derived and related to a uniformly distributed random number set so that a Lehmer pseudorandom number generator could be used for selection of parameter values in the simulations.

The directional surface reflectivity of the fused quartz was modeled successfully by using the complex form of Fresnel's equations. The complex form was used because fused quartz exhibits a complex index of refraction in spectral regions where the material is significantly absorbing. The transmittance of fused quartz was treated as band pass, and it was assumed that within the transitting band the quartz interfaces are totally reflecting/transmitting, while outside of this band the interfaces are totally reflecting/absorbing. Spectral variation of these properties was acquired by allowing the indices (refractive and absorptive) to vary with wavelength in Fresnel's equations. Bulk absorption was spectral in a similar manner and was modeled with the usual extinction coefficient.

Four heating systems were analyzed, including a single lamp with no reflector; a single lamp with a flat reflector; a single lamp with a parabolic reflector; and up to six lamps in a six-lamp, single-reflector heating unit. An experimental apparatus was built to test the various heating systems in an environment where the effect of the surroundings and the test area could be neglected. Distributions of radiant heat flux were recorded from each heating system by traversing a Gardon-type heat flux sensor in the target plane along lines parallel to the two axes of each heating system. This work has shown that the assumptions

regarding the operation of the sensor were reasonble for these applications.

It was found that the source augmentation present in the experiments, because of reflection and the contribution from other sources, could be modeled in the simulation in a simple manner. It was also found that the unradiated power losses from a single unreflected lamp were negligibly small. This result was also observed for systems involving multiple lamps and a reflector. Thus, the nominal electrical power measured for a single lamp, in the heating system of concern, can be used to normalize the simulated predictions for that system.

The simulated results for the single, unreflected lamp case compare very well with the experimental measurements. However, it was found that *importance sampling* would be very beneficial for analysis of such systems, which exhibit large probability of inconsequential process outcomes.

The experimental and simulated results for a system consisting of a single lamp and a flat reflector also show close agreement. Although the reflector was not cooled, the contribution to the radiant field due to reflector reradiation was shown to be negligible. Five simplified simulation models of the system were created to investigate the effects of a variety of modeling issues. These simplified models showed that, although the interactions between the lamp and the reflector were fairly modest for this case, the experimental results exhibited effects of the higher order phenomena, including specular shadowing, quartz transmission (and refraction) of reflected radiation, and source energy distribution sensitivity. It was also found that the lamp filament and quartz tube must both be modeled and allowed to interact in the simulations. The refractive properties of the fused quartz were primarily responsible for distortions in the heat flux distribution, although energy absorption effects were also significant. Therefore, it was concluded that these model refinements were required for accurate analysis and design of most quartz heating systems that utilize reflectors.

The comparisons for a single lamp with a parabolic reflector and a single lamp at various locations in a multilamp unit showed good agreement, but the results indicate that the systems with curved reflectors were very sensitive to configuration geometry. It was demonstrated that the minor discrepancies in some of the correlations were due most probably to inaccuracies in the simulation model of the real system geometries. Since the studied systems with curved reflectors were predominantly specular, they were even sensitive to reflector contour slope inaccuracies. It was found that the sensitivity of these systems to this effect decreased with increasing characteristic distances between the source and the curved reflector, since these radiation sources asymptotically approach line sources at very large distances. Conversely, it was concluded that these effects may be very significant when the characteristic separation distances approach the lamp diameter dimension. The analysis of systems for which lamps with small characteristic distances are dominant (e.g., the parabolic reflector system) will require precise compensation (experimental and/or analytical) for such geometric inaccuracies in order to achieve improved predictions. However, the present study has shown that good agreement is achieved to within the geometrical accuracy.

Predictions of the radiant heat flux distribution produced by a complete six-lamp unit compared very well with the measured distributions. This test case exhibited a significant heat flux contribution due to multiple source enhancement. This effect was quantified by comparing the distributions resulting from the six-lamp case with distributions generated by superimposing single lamp results. It was found that the relative placement of multiple lamps improved the efficiency of the heating unit by concentrating a larger percentage of the available energy within the limits of the target area. The relative enhancement was measured as a function of the number of lamps and was found to increase monotonically from the reference case with a single lamp to a maximum with six lamps, as expected. It was also shown that the increase in relative enhancement approached a maximum asymptotically.

Experiments were run to quantify the effect of a fused-quartz window and its associated forced air cooling on the resulting heat flux distributions for the multilamp heating unit. It was determined that the window and cooling airflow reduced the incident heat flux levels appreciably but did not affect the normalized distributions. The effects of the fused-quartz window and forced air cooling were successfully modeled in the simulation by simple procedures.

This analysis has attempted to encompass basic geometries for quartz heating units that are available commercially and are encountered in practical applications. If system parameters such as geometry, power supply, and material properties are known, this analysis technique can be applied readily to determine a good estimate of the expected heat flux distribution for use in related analyses or during the design process.

Table I. Fractional Function of the First Kind (ref. 27)

[Equation (15)]

λT	$F(\lambda, T)$	λT	$F(\lambda, T)$	λT	$F(\lambda, T)$
1000	0	7 200	0.4809	13 400	0.8317
1200	0	7 400	.5007	13 600	.8370
1400	0	7 600	.5199	13 800	.8421
1600	.0001	7 800	.5381	14 000	.8470
1800	.0003	8 000	.5558	14 200	.8517
2000	.0009	8 200	.5727	14 400	.8563
2200	.0025	8 400	.5890	14 600	.8606
2400	.0053	8 600	.6045	14 800	.8648
2600	.0098	8 800	.6195	15 000	.8688
2800	.0164	9 000	.6337	16 000	.8868
3000	.0254	9 200	.6474	17 000	.9017
3200	.0368	9 400	.6606	18 000	.9142
3400	.0506	9 600	.6731	19 000	.9247
3600	.0667	9 800	.6851	20 000	.9335
3800	.0850	10 000	.6966	21 000	.9411
4000	.1051	10 200	.7076	22 000	.9475
4200	.1267	10 400	.7181	23 000	.9531
4400	.1496	10 600	.7282	24 000	.9589
4600	.1734	10 800	.7378	25 000	.9621
4800	.1979	11 000	.7474	26 000	.9657
5000	.2229	11 200	.7559	27 000	.9689
5200	.2481	11 400	.7643	28 000	.9718
5400	.2733	11 600	.7724	29 000	.9742
5600	.2983	11 800	.7802	30 000	.9765
5800	.3230	12 000	.7876	40 000	.9881
6000	.3474	12 200	.7947	50 000	.9941
6200	.3712	12 400	.8015	60 000	.9963
6400	.3945	12 600	.8081	70 000	.9981
6600	.4171	12 800	.8144	80 000	.9987
6800	.4391	13 000	.8204	90 000	.9990
7000	.4604	13 200	.8262	100 000	.9992
				∞	1.0000

Table II. Spectral Real-Refractive and Absorptive Indices of Fused Quartz (ref. 28)

λ, μm	η_q	κ_q	λ, μm	η_q	κ_q	λ, μm	η_q	κ_q
0.2138	1.53426	0	1.6932	1.44225	0	9.30	2.35	2.4400
.2144	1.53370	0	1.7091	1.44206	0	9.35	2.50	2.2100
.2267	1.52281	0	1.8130	1.44069	0	9.40	2.76	1.3700
.2302	1.52005	0	1.9700	1.43853	0	9.50	2.98	1.5200
.2378	1.51475	0	2.0581	1.43721	0	9.60	3.00	1.2100
.2399	1.51336	0	2.3254	1.43292	0	9.70	2.98	.9000
.2482	1.50839	0	2.4374	1.43093	0	9.80	2.87	.6100
.2652	1.50000	0	3.2439	1.41314	0	9.90	2.77	.4100
.2698	1.49804	0	3.2668	1.41253	0	10.00	2.62	.2804
.2752	1.49592	0	3.3026	1.41156	0	10.20	2.36	.1900
.2803	1.49403	0	3.4220	1.40822	0	10.40	2.22	.1400
.2893	1.49101	0	3.5070	1.40565	0	10.60	2.00	.1210
.2967	1.48872	0	3.5564	1.40414	0	10.80	1.99	.1330
.3021	1.48719	0	3.7067	1.39937	0	11.00	1.93	.1430
.3302	1.48054	0	5.0000	1.30000	0	11.20	1.89	.1620
.3341	1.47976	0	6.0000	1.20000	0	11.40	1.84	.1900
.3403	1.47858	0	7.0000	1.05000	.0137	11.60	1.79	.1980
.3466	1.47745	0	7.1000	1.04000	.0139	11.80	1.73	.2210
.3610	1.47512	0	7.2000	1.02000	.0144	12.00	1.71	.2600
.3650	1.47452	0	7.3000	1.00000	.0160	12.20	1.72	.3200
.4046	1.46961	0	7.4000	.96000	.0187	12.40	1.80	.3600
.4358	1.46669	0	7.5000	.93000	.0250	12.60	1.87	.3650
.4678	1.46429	0	7.6000	.90000	.0365	12.80	1.98	.3250
.4861	1.46313	0	7.7000	.83000	.0560	13.00	1.95	.2500
.5085	1.46186	0	7.8000	.76000	.0750	13.20	1.91	.1940
.5460	1.46007	0	7.9000	.64500	.1140	13.40	1.89	.1400
.5769	1.45884	0	8.0000	.50000	.2500	13.60	1.84	.1050
.5790	1.45877	0	8.1000	.37400	.3950	13.80	1.79	.0820
.5875	1.45846	0	8.2000	.38000	.5570	14.00	1.76	.0800
.5892	1.45840	0	8.3000	.41700	.6300	14.20	1.73	.0800
.6438	1.45670	0	8.4000	.45000	.7800	14.40	1.71	.0800
.6562	1.45637	0	8.5000	.44800	.8600	14.60	1.68	.0800
.6678	1.45607	0	8.6000	.43300	.9700	16.00	1.48	.1220
.7065	1.45515	0	8.6500	.42000	1.0500	18.00	1.26	.2750
.8521	1.45246	0	8.7000	.39000	1.1500	19.00	1.02	.3880
.8943	1.45184	0	8.7500	.37000	1.2400	20.00	.64	.8700
1.0139	1.45024	0	8.8000	.33000	1.3500	20.50	.52	1.5200
1.0829	1.44940	0	8.8500	.32000	1.5000	21.00	1.30	2.3700
1.1286	1.44887	0	8.9000	.33600	1.6500	21.50	2.24	2.1100
1.3622	1.44619	0	8.9500	.46000	2.1000	22.00	2.59	1.7200
1.3950	1.44584	0	9.0000	.74000	2.4400	23.00	2.77	1.0400
1.4695	1.44498	0	9.0500	1.14000	2.7100	24.00	2.75	.6100
1.5295	1.44427	0	9.1000	1.64000	2.3000	26.00	2.60	.2800
1.6606	1.44265	0	9.1500	1.95000	2.8100			
1.6810	1.44240	0	9.2000	2.20000	2.5500			

Table III. Estimated Spectral Reflectivity and Emissivity Data

(a) Spectral reflectivity components of a polished titanium reflector*

λ, μm	ρ_s	ρ_d
0	0	0
.200	.035	.015
.310	.085	.205
.422	.185	.315
.534	.260	.280
.646	.315	.270
.758	.360	.270
.870	.450	.210
1.150	.510	.160
1.420	.575	.105
1.690	.620	.070
1.960	.665	.030
2.230	.690	.010
26.000	1.000	.000

*Measured by R. E. Wright, Jr., at NASA Langley Research Center.

(b) Estimated hemispherical emissivity of fused quartz from $\epsilon = \int_0^\infty 0.8\epsilon_{\lambda n}\, d\lambda$ (ref. 27)

Temperature, K	ϵ
295	0.90
500	.40
1000	.50
1500	.30
2000	.20
2500	.14

Appendix

Detailed Simulation Flowchart Corresponding to Single-Lamp, Flat-Reflector System

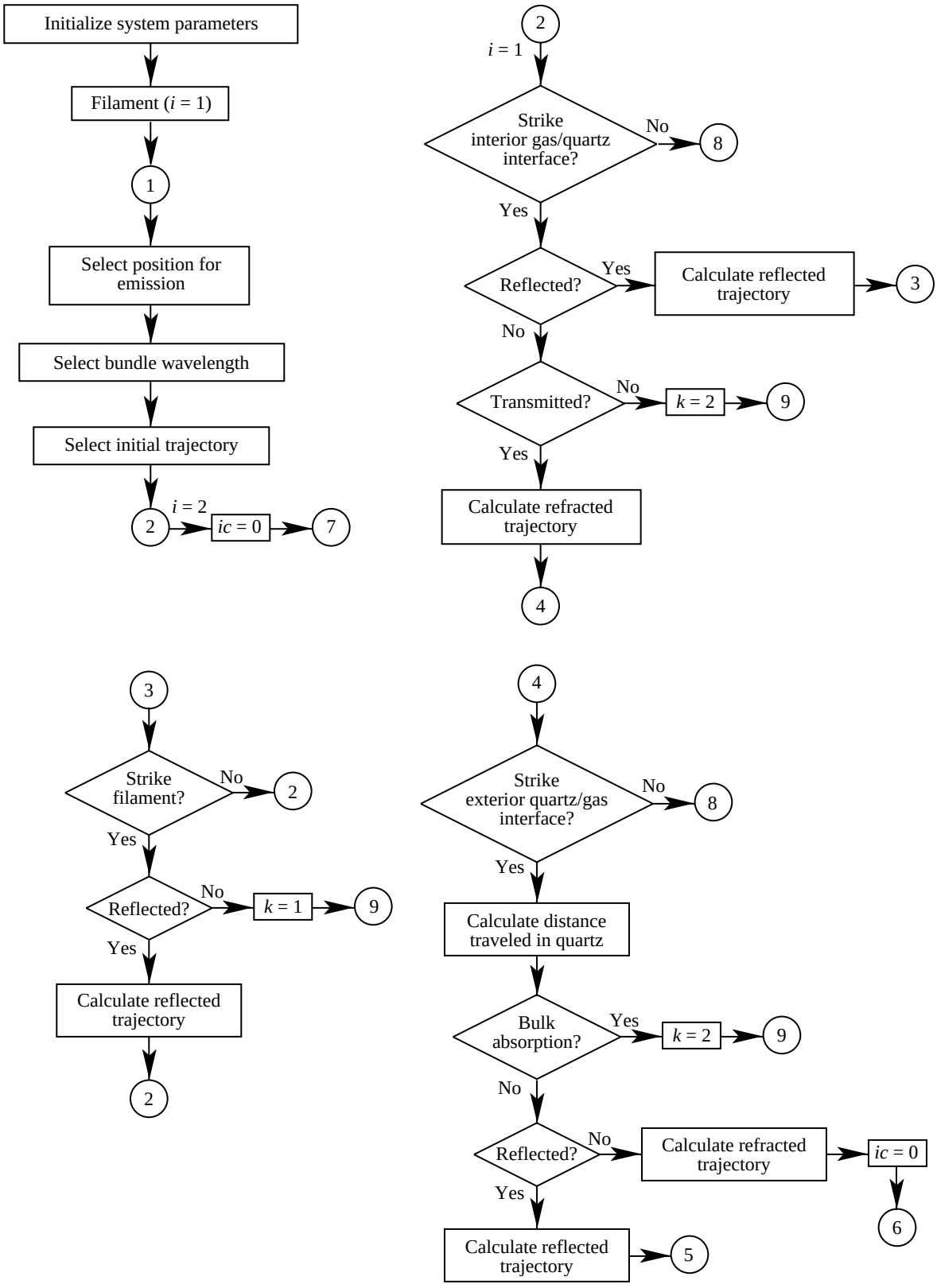

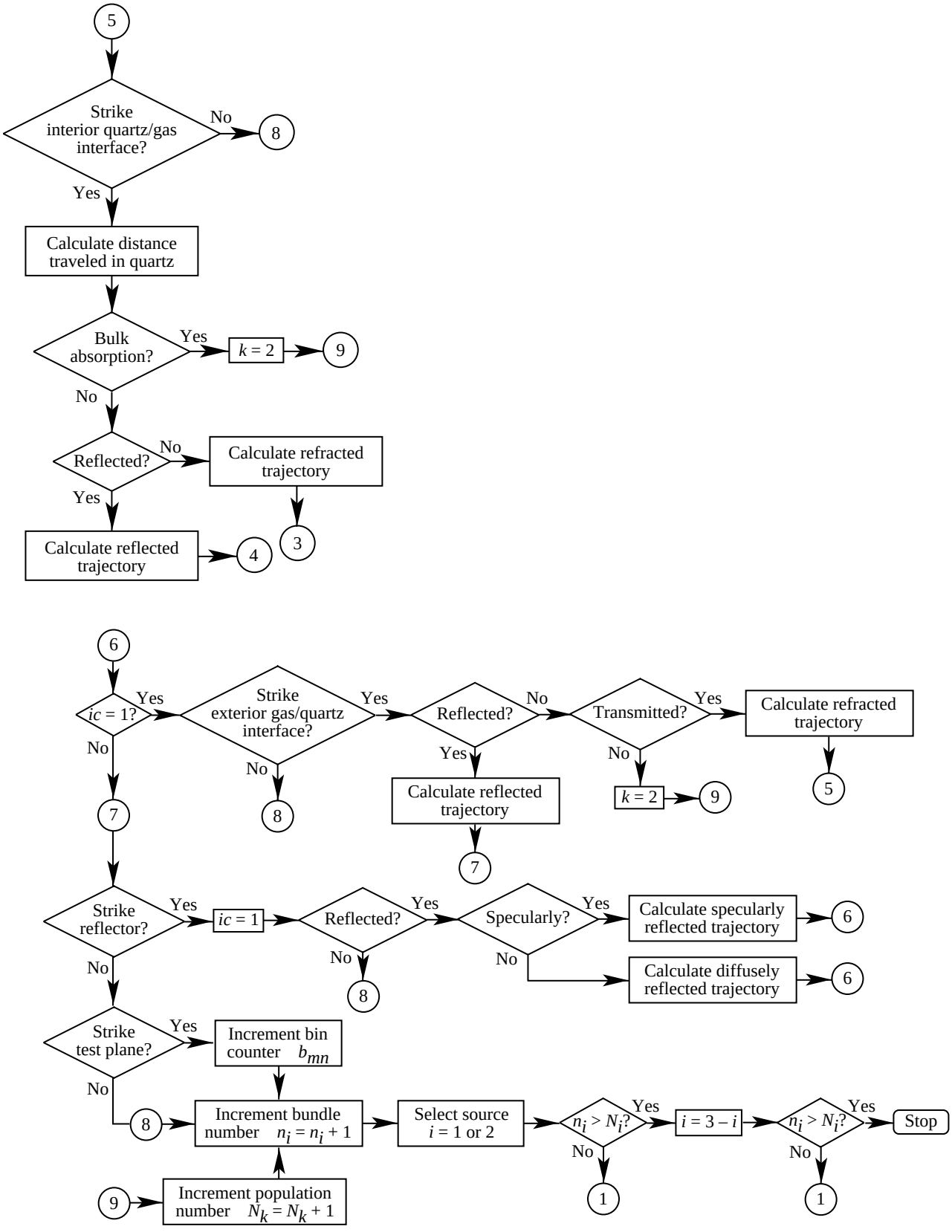
5
Strike interior quartz/gas interface?
No
8
Yes
Calculate distance traveled in quartz
Bulk absorption?
Yes
k = 2
9
No
Reflected?
No
Calculate refracted trajectory
Yes
3
Calculate reflected trajectory
4
6
ic = 1?
Yes
Strike exterior gas/quartz interface?
Yes
Reflected?
No
Transmitted?
Yes
Calculate refracted trajectory
No
Yes
No
5
8
Calculate reflected trajectory
k = 2
9
7
7
Strike reflector?
Yes
ic = 1
Reflected?
Yes
Specularly?
Yes
Calculate specularly reflected trajectory
6
No
No
8
No
Calculate diffusely reflected trajectory
6
Strike test plane?
Yes
Increment bin counter b_mn
No
8
Increment bundle number n_i = n_i + 1
Select source i = 1 or 2
n_i > N_i?
Yes
i = 3 – i
n_i > N_i?
Yes
Stop
No
No
1
1
9
Increment population number N_k = N_k + 1

References

1. Hanson, H. A.; and Casey, J. J.: *High Temperature Test Technology* AFWAL-TR-86-3105, U.S. Air Force, Feb. 1987. (Available from DTIC as AD A179 932.)

2. Ash, Robert L.: *An Analysis of the Radiation Field Beneath a Bank of Tubular Quartz Lamps.* NASA CR-191551, 1972.

3. Turner, Travis L.; and Ash, Robert L.: *Prediction of the Thermal Environmental and Thermal Response of Simple Panels Exposed to Radiant Heat.* NASA TM-101660, 1989.

4. Turner, T. L.; and Ash, R. L.: Analysis of the Thermal Environment and Thermal Response Associated With Thermal-Acoustic Testing. *A Collection of Technical Papers, Part 2—31st AIAA/ASME/ASCE/AHS/ASC Structures, Structural Dynamics and Materials Conference*, Apr. 1990, pp. 824–830. (Available as AIAA-90-0975.)

5. Kahn, Herman: *Applications of Monte Carlo.* Res. Memo. AECU-3259 (Contract No. AT(11-3)-135), Rand Corp., 1956.

6. Cashwell, E. D.; Everett, C. J.; and Rechard, O. W.: *A Practical Manual on the Monte Carlo Method for Random Walk Problems.* LA-2120 (Contract W-7405-ENG. 36), Univ. of California, Dec. 18, 1957.

7. James, F.: Monte Carlo Theory and Practice. *Rep. Prog. Phys.*, vol. 43, Sept. 1980, pp. 1145–1189.

8 Turner, Travis Lee: Simulation and Measurement of the Radiant Field Produced by Quartz Heating Systems. M.S. Thesis, Old Dominion Univ., July 1991.

9. Howell, J. R.; and Perlmutter, M.: Monte Carlo Solution of Thermal Transfer Through Radiant Media Between Gray Walls. *J. Heat Transf.*, vol. 86, no. 1, Feb. 1964, pp. 116–122.

10. Perlmutter, M.; and Howell, J. R.: Radiant Transfer Through a Gray Gas Between Concentric Cylinders Using Monte Carlo. *J. Heat Transf.*, vol. 86, no. 2, May 1964, pp. 169–179.

11. Howell, John R.; and Perlmutter, Morris: Monte Carlo Solution of Radiant Heat Transfer in a Nongrey Nonisothermal Gas With Temperature Dependent Properties. *A.I.Ch.E. J.*, vol. 10, no. 4, July 1964, pp. 562–567.

12. Howell, John R.; Strite Mary Kern; and Renkel, Harold: Heat-Transfer Analysis of Rocket Nozzles Using Very High Temperature Propellants. *AIAA J.*, vol. 3, no. 4, Apr. 1965, pp. 669–673.

13. Howell, John R.: *Calculation of Radiant Heat Exchange by the Monte Carlo Method.* NASA TM X-52101, 1965.

14. Siegel, R.; and Howell, J. R.: *Thermal Radiation Heat Transfer.* McGraw-Hill, Inc., 1972.

15. Murakami, Masahide: Direct Monte Carlo Simulation of Two-Dimensional Radiative Heat Transfer in Absorbing-Emitting Medium Bounded by the Nonisothermal Gray Walls. *Proceedings of the Ninth International Symposium on Space Technology and Science*, AGNE Publ., Inc., 1971, pp. 407–416.

16. Weiner, M. M.; Tindall, J. W.; and Candell, L. M.: Radiative Interchange Factors by Monte Carlo. ASME Paper 65-WA/HT-51, Nov. 1965.

17. Corlett, R. C.: Direct Monte Carlo Calculation of Radiative Heat Transfer in Vacuum. *J. Heat Transf.*, vol. 88, Nov. 1966, pp. 376–382.

18. Toor, J. S.; and Viskanta, R.: A Numerical Experiment of Radiant Heat Interchange by the Monte Carlo Method. *Int. J. Heat & Mass Transf.*, vol. 11, 1968, pp. 883–897.

19. Mahan, J. R.; and Eskin, L. D.: The Radiation Distribution Factor—Its Calculation Using Monte Carlo Techniques and an Example of Its Application. *First U.K. National Conference on Heat Transfer*, Symp. Ser. No. 86, Inst. of Chemical Engineers (British), 1984, pp. 1001–1012.

20. Hoff, S. J.; and Janni, K. A.: Monte Carlo Technique for the Determination of Thermal Radiation Shape Factors. *Trans. American Soc. Agric. Eng.*, vol. 32, no. 3, May–June 1989, pp. 1023–1028.

21. Chou, Tien S.: A Monte Carlo Approach to Optical Analysis. *Opt. Eng.*, vol. 13, no. 4, July–Aug. 1974, pp. 299–302.

22. Morris, P. A.; James, R. K.; McMurrin, J. C.; Felland, J. R.; Edwards, D. K.; and Buchberg, H.: Radiative Transfer Through Thin-Walled Glass Honeycomb. ASME Paper 76-HT-48, Aug. 1976.

23. Naraghi, M. H. N.; and Chung, B. T. F.: A Stochastic Approach for Radiative Exchange in Enclosures with Non-Participating Medium. ASME Paper 83-HT-52, July 1983.

24. Rasmussen, N. B. Kampp; Torslev, P.; and Hadvig, S.: Numerical Integration Method of Radiative Exchange (NIMREX). *Int. J. Heat & Mass Transf.*, vol. 32, no. 2, 1989, pp. 343–350.

25. Park, Stephen K.; and Miller, Keith W.: Random Number Generators: Good Ones Are Hard To Find. *Comput. Pract.*, vol. 31, no. 10, Oct. 1988, pp. 1192–1201.

26. Ozisik, M. N.: *Radiative Transfer and Interactions With Conduction and Convection.* John Wiley & Sons, Inc., 1980.

27. Touloukian, Y. S.; and Ho, C. Y.: *Thermophysical Properties of Selected Aerospace Materials. Part 1—Thermal Radiative Properties.* Hemisphere Publ. Corp., 1976.

28. Touloukian, Y. S.; and DeWitt, D. P., eds.: *Thermal Radiative Properties—Nonmetallic Solids.* IFI/Plenum, 1972.

29. Lang, M. L.; and Wolfe, William L.: Optical Constants of Fused Silica and Sapphire From 0.3 to 25 μm. *Appl. Opt.*, vol. 22, no. 9, May 1983, pp. 1267–1268.

30. Hsieh, C. K.; and Su, K. C.: Thermal Radiative Properties of Glass From 0.32 to 206 μm. *Sol. Energy,* vol. 22, no. 1, 1979, pp. 37–43.

31. Drummeter, Louis F., Jr.; and Hass, Georg: Solar Absorptance and Thermal Emittance of Evaporated Coatings. *Physics of Thin Films*, Volume 2, Academic Press, 1964, pp. 305–361.

32. Malone, Erle W.: *Design and Calibration of Thin Foil Heat Flux Sensors.* Preprint No. P6-2-PHYMMID-67, Instrument Soc. of America, 1967.

33. Ash, R. L.; and Wright, R. E., Jr.: Design Considerations for Gardon Heat Flux Sensors. AIAA Paper No. 71-470, Apr. 1971.

REPORT DOCUMENTATION PAGE

Form Approved
OMB No. 0704-0188

1. AGENCY USE ONLY *(Leave blank)*	2. REPORT DATE	3. REPORT TYPE AND DATES COVERED
	March 1994	Technical Paper

4. TITLE AND SUBTITLE
Numerical and Experimental Analyses of the Radiant Heat Flux Produced by Quartz Heating Systems

5. FUNDING NUMBERS
WU 505-63-50-10

6. AUTHOR(S)
Travis L. Turner and Robert L. Ash

7. PERFORMING ORGANIZATION NAME(S) AND ADDRESS(ES)
NASA Langley Research Center
Hampton, VA 23681-0001

8. PERFORMING ORGANIZATION REPORT NUMBER
L-17081

9. SPONSORING/MONITORING AGENCY NAME(S) AND ADDRESS(ES)
National Aeronautics and Space Administration
Washington, DC 20546-0001

10. SPONSORING/MONITORING AGENCY REPORT NUMBER
NASA TP-3387

11. SUPPLEMENTARY NOTES
Turner: Langley Research Center, Hampton, VA
Ash: Old Dominion University, Norfolk, VA

12a. DISTRIBUTION/AVAILABILITY STATEMENT
Unclassified–Unlimited

Subject Category 71

12b. DISTRIBUTION CODE

13. ABSTRACT *(Maximum 200 words)*

A method is developed for predicting the radiant heat flux distribution produced by tungsten filament, tubular fused-quartz envelope heating systems with reflectors. The method is an application of Monte Carlo simulation, which takes the form of a random walk or ray tracing scheme. The method is applied to four systems of increasing complexity, including a single lamp without a reflector, a single lamp with a flat reflector, a single lamp with a parabolic reflector, and up to six lamps in a six-lamp contoured-reflector heating unit. The application of the Monte Carlo method to the simulation of the thermal radiation generated by these systems is discussed. The procedures for numerical implementation are also presented. Experiments were conducted to study these quartz heating systems and to acquire measurements of the corresponding empirical heat flux distributions for correlation with analysis. The experiments were conducted such that several complicating factors could be isolated and studied sequentially. Comparisons of the experimental results with analysis are presented and discussed. Good agreement between the experimental and simulated results was obtained in all cases. This study shows that this method can be used to analyze very complicated quartz heating systems and can account for factors such as spectral properties, specular reflection from curved surfaces, source enhancement due to reflectors and/or adjacent sources, and interaction with a participating medium in a straightforward manner.

14. SUBJECT TERMS	15. NUMBER OF PAGES
Heating equipment; Quartz lamps; Radiant heating; Thermal radiation; Infrared radiation; Heat flux; Radiative heat transfer; Monte Carlo method; Ray tracing; Numerical simulation; Random sampling; Photons	38
	16. PRICE CODE A03

17. SECURITY CLASSIFICATION OF REPORT	18. SECURITY CLASSIFICATION OF THIS PAGE	19. SECURITY CLASSIFICATION OF ABSTRACT	20. LIMITATION OF ABSTRACT
Unclassified	Unclassified		